STATISTICAL ANALYSIS OF ROCK FABRICS

by

BORIS AVDEEV

Presented to the Faculty of the Graduate School of

The University of Texas at Arlington in Partial Fulfillment

of the Requirements

for the Degree of

MASTER OF SCIENCE IN GEOLOGY

THE UNIVERSITY OF TEXAS AT ARLINGTON

August 2005

ACKNOWLEDGEMENTS

I would like to thank my supervising professor Dr. John Wickham for his valuable help with my work, constant motivation and encouragement with the aid of deadlines and for his incredible belief in my well timed success.

I wish to express my deep appreciation to Dr. Doyle Hawkins for his interest in my research, great aid with it and his tremendous patience regarding my statistical ignorance.

I cannot forget Dr. Merlynd Nestell who agreed to be a committee member for my thesis regardless of his antagony of statistics together with structural geology. Also I would like to thank him for his help with me "staying out of trouble" without which I doubt I would be able to reach this point of my graduate studies in the United States. I ought to mention Dr. Galina Nestell whose coffee kept me up during early afternoons.

I am grateful to Elisabeth Ballard and Patricia Cowan who helped me to meet (or fight) various school deadlines.

Also I would like to acknowledge R developers (`http://www.r-project.org/`) for providing a great open source statistical computing environment.

Finally I thank everybody else who deserved it but was remembered about only after this document had been printed.

July 13, 2005

ABSTRACT

STATISTICAL ANALYSIS OF ROCK FABRICS

Publication No. _____

Boris Avdeev, M.S.

The University of Texas at Arlington, 2005

Supervising Professor: John Wickham

The main goal of the work is to present new procedures for statistical analysis of fabric data for structural geology. After an introduction to the problems of orientation analysis, discussion of different types of the orientation data and a brief review of the existing techniques and statistics for the orientation data, a comprehensive discussion of several proposed methods is given.

The first part of the methodology chapter states a general model in terms of a structural frame and introduces some notation. The second part is a detailed description of a pooled estimator, which is intended to assess a structural frame mean orientation using different sorts of data simultaneously. The third part is a discussion of a regression model in a transformed space. Four sub-models are derived and a method for fitting is provided. This chapter ends with a brief coverage of a problem of spatial autocorrelation.

Next chapter presents a sample analysis of the Kukas lake structure of the Baltic shield, North West Russia. This dataset is analized by all the models. The obtained trends and orientations are plotted in various ways. A residual analysis for the models closes the chapter.

TABLE OF CONTENTS

LIST OF ILLUSTRATIONS

LIST OF TABLES

CHAPTER 1

INTRODUCTION

Orientation analysis, one of the branches of structural geology, studies strain related rock fabrics aiming to obtain some information about the stress-strain conditions responsible for the appearance of these textures. The basic principle of orientation analysis is that the orientation of each fabric is determined by the stress and strain fields. Therefore by studying textures one can constrain past stress-strain conditions.

Many researches have studied the problem of stress-strain-fabric orientation relationships (Hanmer & Passchier, 1991, Nicolas, 1987, Karato & Wenk, 2002, Turner & Weiss, 1963). Indeed, knowledge of these relationships is a key to orientation analysis. However, to properly use this information one needs effective statistical techniques to extract important parts from necessarily noisy field observations. Surprisingly, this aspect of the problem has been investigated by structural geologists to much less extent.

The purpose of this work is to introduce several techniques for quantitative fabric data analysis and discuss some problems that need to be solved by future research.

In the current chapter I am going to present some background on orientation analysis, spherical and spatial statistics, and give a brief review of current state of research in the contributing sciences.

In chapter 2, I will describe the proposed methods and also mention once again the existing techniques, that may be familiar to statisticians but seem to be not so well known by geologists.

Chapter 3 contains a detailed example on the analysis of fabric data from the Kukas lake area of the Baltic shield. This analysis shows the utility of the proposed techniques as

well as their problematic spots. Some discussion and geological interpretation follows the analysis. This chapter is intended to show the value of this work for structural geology.

Finally in chapter 4 the current work is summarized to give clear perception of its position in the body of structural geology and orientation analysis. Based on chapter 3, conclusions on usability are provided. At last, directions of further study are discussed.

1.1 Orientation Data

For purposes of orientation analysis, a rock fabric is understood as some specific orientation in a rock with respect to a geographical coordinate system or any other suitable frame of reference. Fabric orientation can be defined by a preferred orientation of non-isometric crystals, attitude of composition boundaries such as bedding planes in sedimentary rocks and a bending in metamorphic or igneous rocks, orientation of deformed pebbels in a conglomerate, specific direction of folds and so on. From the mathematical point of view there are several distinguishable types of fabric element orientations, which I will discuss in the following three sections.

1.1.1 Directions

The first type of orientation is a direction in a q-dimentional real vector space $\mathbb{R}^q$. Those are usually represented by unit vectors and therefore this type of data can be seen as points on a $(q-1)$ dimensional unit sphere (hence orientation data is sometimes referred to as spherical data). This type of data is said to belong to a Stiefel manifold[1] $S^{1,q}$. Another possible representation is by $(q-1)$ Euler angles. They are used most

[1] Stiefel manifold, denoted $S_k(V^n)$ or $S^{k,n}$, is the set of all orthonormal k-frames in n-dimentional vector space V.

often in field geology to write down the fabric attitudes. Conversion between the Euler angles and the $\mathbb{R}^3$ vector representation is provided by

$$d_1 = \cos\theta\cos\phi \tag{1.1a}$$

$$d_2 = \sin\theta\cos\phi \tag{1.1b}$$

$$d_3 = \sin\phi, \tag{1.1c}$$

where d_i are components of the $\mathbb{R}^3$ vector, θ is a longitude (or trend) and ϕ is a latitude (or plunge). Orthogonal coordinates in $\mathbb{R}^3$ are defined such that the x_1 axis is directed North, x_2 — East and x_3 — down.

Unlike the $\mathbb{R}^q$ unit vector, Euler angles are the minimal representation of $S^{1,q}$. However they are useless in computations and bear singularities at the poles.

A distance measure between two directions is naturally an angle:

$$\theta(\boldsymbol{d}_1, \boldsymbol{d}_2) = \arccos(\boldsymbol{d}_1^T \boldsymbol{d}_2), \tag{1.2}$$

where $\boldsymbol{d}_i$ is the $S^{1,q}$ point represented as a $\mathbb{R}^q$ unit vector.

1.1.2 Axes

The second, and most common type in structural geology, is an unsigned direction usually called an axis. Axes are commonly represented in the same way as the directions. The only difference is that there are two opposite directions d and $-d$ corresponding to every axis l and therefore such representation is not unique. The space of axes is sometimes called $S_+^{1,q}$, which implies that all axes can be presented as points on a unit hemisphere in $\mathbb{R}^q$. However, more precisely, axes are points on a Grassman manifold[2] $G_{1,q}(\mathbb{R}^3)$.

[2] Grassman manifold is the space of all k-dimensional subspaces of an n-dimensional vector space V, often denoted as $G_k(V^n)$ or simply $G^{k,n}$.

The distance between two axes can be expressed as minimum angle between corresponding directions, i.e.

$$\begin{aligned}\theta(\boldsymbol{l}_1, \boldsymbol{l}_2) &= \min\big(\arccos(\boldsymbol{l}_1^T \boldsymbol{l}_2), \arccos(-\boldsymbol{l}_1^T \boldsymbol{l}_2)\big) = \\ &= \arccos |\boldsymbol{l}_1^T \boldsymbol{l}_2|,\end{aligned} \tag{1.3}$$

where $\boldsymbol{l}_i$ is a $G^{1,q}$ axis written as an $\mathbb{R}^q$ vector.

Van den Boogaart & Schaeben (2002a) suggest $\mathbb{R}^{q\times q}$ representation for axes, which can be derived from the $\mathbb{R}^q$ representation as follows

$$f(\boldsymbol{l} \in G^{1,q}) = \boldsymbol{l}\boldsymbol{l}^t = \begin{pmatrix} l_1 l_1 & \cdots & l_1 l_q \\ \vdots & \ddots & \vdots \\ l_q l_1 & \cdots & l_q l_q \end{pmatrix} \mapsto \begin{pmatrix} l_1 l_1 \\ \vdots \\ l_1 l_q \\ \vdots \\ \vdots \\ l_q l_1 \\ \vdots \\ l_q l_q \end{pmatrix} \in \mathbb{R}^{q\times q} \tag{1.4}$$

This representation is convenient because the distance between two axes can be expressed as

$$\theta(\boldsymbol{u}_1, \boldsymbol{u}_2) = \|\boldsymbol{u}_1 - \boldsymbol{u}_2\| = \sqrt{2}\sin\theta(\boldsymbol{l}_1, \boldsymbol{l}_2), \tag{1.5}$$

where $\boldsymbol{u}_i$ is a representation of $\boldsymbol{l}_i$ according to equation (1.4).

1.1.3 Orthogonal Rigid Frames

A generalization of the Stiefel manifold that accounts for more than a single direction is written as $S_r(\mathbb{R}^q)$, where r is is a number of $S^{1,q}$ dimensional orthogonal directions in a so called *rigid frame* which represents a single point on $S_r(\mathbb{R}^q)$. Now the direction is just $S_1(\mathbb{R}^q)$ special case of $S_r(\mathbb{R}^q)$.

Other special cases are $S_q(\mathbb{R}^q)$ q-frames in $\mathbb{R}^q$ space, which is isomorphic to $\mathrm{O}(q)$ orthogonal group, and $S_{q-1}(\mathbb{R}^q)$ isomorphic to $\mathrm{SO}(q)$. Orthogonal group $\mathrm{O}(q)$ is a set of all $q \times q$ orthogonal matrices, while $\mathrm{SO}(q)$ (special orthogonal group) is the same group but limited to matrices with the determinant equal one, i.e. this group does not include improper rotations. Data belonging to these two special cases is usually referred to as *rotational data*.

Analogous generalization exist for axes. Their orthogonal frames are said to belong to a Grassman manifold $G_r(\mathbb{R}^q)$.

For more information on orientations refer to Mardia & Jupp (2000), Altmann (1986).

1.2 Rock Fabrics

As it was mentioned above, in orientation analysis rock fabrics[3] are considered to be just orientations of various types in $\mathbb{R}^3$. The most common fabrics such as lineations, fold axes, normals to bedding and foliation planes are treated as axes since in most cases they don't possess any directional information. However, in case where one can recognize sedimentary structures in layers to tell upright or overturned orientation of the bedding or sense of shear in case of foliation and lineation, corresponding orientations should be considered as directions.

Lineation and foliation often occur together in the same structural paragenesis, i.e. they correspond to the same deformation event. In this case foliation-lineation pairs can be treated as a rigid frame on either Stiefel or Grassman manifold.

A combination of different types of fabrics can be used to define a *structural frame*. Consider cylindrical folds of bedding and a corresponding fold axis lineation (figure 1.1).

[3] In this work the term *fabric* is used in narrow sense, i.e. it stands for an atomic (in a scale of observation) texture element. The wide sense fabric will be called a *structural frame* and is discussed below.

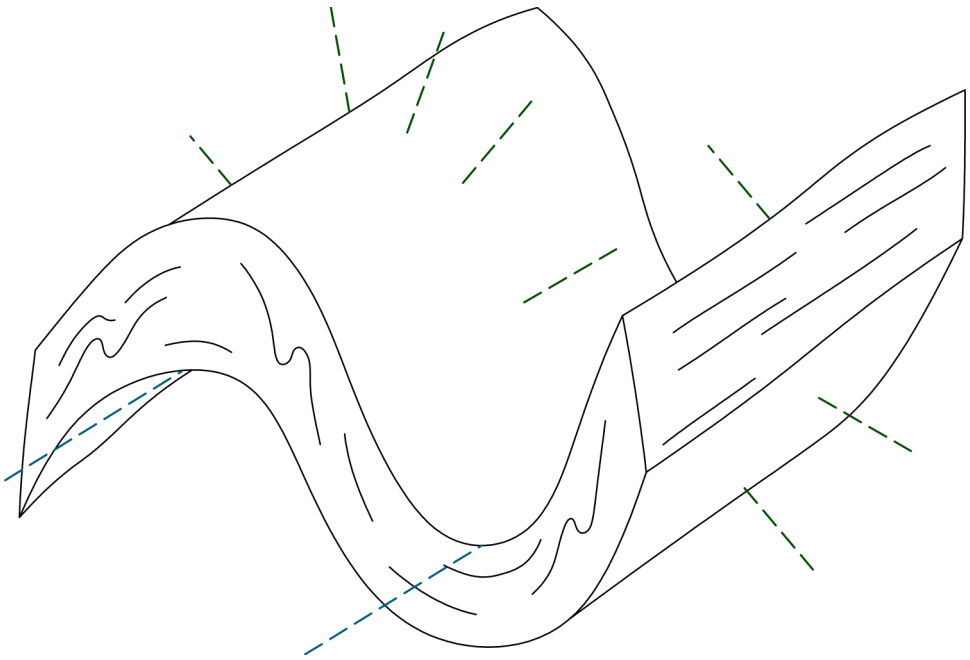

Figure 1.1 Structural paragenesis of a cylindrically folded domain.

Providing that the lineation is parallel to the fold axes, both the fold axes and lineation can be grouped together and called b-fabrics related to a β axis of the structural frame. Often, this β axis may correspond further to a medium eigenvalue eigenvector of the strain tensor. If an axial plane cleavage is present, its normal will define the α axis of the structural frame. This α axis will usually be interpreted as the direction of maximum compressional strain.

The structural frame provides a convenient abstraction for the fabric data. It serves as a middle-tier layer between the field observation and their interpretation in terms of strain or stress.

1.3 Statistical Distributions and Analysis Methods for Orientation Data

Each of the types of spherical data has been treated by several authors. The most comprehensive and up to date text on this subject is a book by Mardia & Jupp (2000). Other significant references are Fisher et al. (1993) and Watson (1983).

Most attention was given to directional data. There exist a number of theoretical distributions and many inference procedures for this type of data. Original research on this topic was done by Presnell et al. (1998), Fisher et al. (1996), Fisher & Hall (1989), Jupp & Mardia (1989), Rivest (1989), Ducharme & Milasevic (1987), Jupp (1987), Ducharme (1985), Jupp & Spurr (1983), Kent (1982), Jupp & Mardia (1980), Beran (1979), Wellner (1979), Bingham & Mardia (1978), Prentice (1978) and Mardia (1975). The main topics of these papers include distribution theory, miscellaneous single and multiple sample parametric and non-parametric tests and so on. Much less attention was paid to the regression techniques with the exception of spherical-spherical regression (Procrustes analysis). Kriging techniques for the directional data are discussed in light of injective embedding transformation into $\mathbb{R}^q$ in van den Boogaart & Schaeben (2002a), Young (1987b,a).

Axial data is covered to much less extent. However in most cases it should not be too challenging to modify the techniques of the directional statistics to fit axial data. Besides the textbooks mentioned, published research relevant to this topic include Kunze & Schaeben (2004), Wood (1993), Kent (1987), Tyler (1987), Wood (1987), Prentice (1984), Kent (1982), Wood (1982), Bingham (1974). Kriging for axial data is covered by van den Boogaart & Schaeben (2002a).

Vollmer (1990) discusses a technique for subdividing a region into a number of domains with more or less high *cylindricity* inside each domain. By cylindricity he means a goodness of fit of the c-fabrics to a great circle.

This method can be called a spatially supervised spherical classification. Its main application is an automated domain search in computer aided geological mapping.

CHAPTER 2

METHODOLOGY

In this chapter I am going to present a model and methods for the analysis of orientation data in structural geology.

The structural frame mentioned in the introduction and used in the rest of this paper will contain only one axis which I will call a β structural axis.

This axis will correspond to such fabrics as a β-lineation and fold axes (b-structures). This means that in terms of kinematics the β-axis may coincide with the intermediate eigenvector of the strain tensor.

Another set of fabrics including bedding or pre-existing foliation is assumed to be deformed in cylindrical folds in the same strain field which is responsible for the appearance of the b-structures. These folded fabric elements (called c-fabrics) will be distributed along a great circle normal to the average direction of the b-fabrics, parallel to the β axis.

Such a model describes many data sets in structural geology. Some data sets can be studied with some straightforward adjustments.

The main consequence of this model is that the β axis can be estimated using both kinds of fabrics. In the next sections I will elaborate on this, but before that let me introduce some notation.

Let A be $n \times 3$ matrix of measurements of a-type fabrics represented as unit vectors in $\mathbb{R}^3$. Then its *scatter matrix*, also known as *orientation tensor* or *Scheidegger tensor* is defined as

$$L^a = n^{-1} A^T A, \tag{2.1}$$

where A^T means transposition of A (Woodcock, 1977, Lisle, 1985).

Further let $\lambda_1^{L^a} \geq \lambda_2^{L^a} \geq \lambda_3^{L^a} \geq 0$ be eigenvalues of L^a and $\upsilon_1^{L^a}, \upsilon_2^{L^a}, \upsilon_3^{L^a}$ corresponding eigenvectors. It can be shown that trace of $A^T A$ is n, therefore

$$\sum_{i=1}^{3} \lambda_i^{L^a} = 1. \tag{2.2}$$

Unlike the scatter matrix of linear data, L incorporates both spherical location parameter[1] and scatter of the sample. The former is determined by eigenvectors and the later by eigenvalues.

2.1 Pooled Estimator $\beta^{b,c}$

According to the model described in the beginning of this chapter, the β-axis can be estimated using both, b- and c-fabrics. Since these two types of fabric often co-exist, it is important to be able to estimate β-axis using both types of data simultaneously.

When for each measurement of one type there is a corresponding measurement of another type, both measurements can be considered as components of a single observation. A pair of b- and c-structures can be thought of as a rigid frame, which can be treated as a point on Grassman manifold. There are a number of statistical distributions and procedures designed for such kind of data. For more details refer to Downs (1972), Bingham (1974), Khatri & Mardia (1977), Bingham & Mardia (1978), Jupp & Mardia (1979), de Waal (1979), Bingham et al. (1992), Purkayastha & Mukerjee (1992), Wood (1993), Mardia & Jupp (2000).

In case of a few missing components of an observation, the observation can be simply omitted or, alternatively, the missing part of the observation can be guessed by virtue of imputation. However when the proportion of missing data becomes significant,

[1] The term *location* is used by analogy with the linear data. Although in case of orientation data more naturally this value should be called an *orientation* of a distribution, word "orientation" is already reserved for the type of data. Therefore these two meanings would interfere with awkwardly in speech and text (e.g. re-read this footnote).

neither solution is satisfactory: imputation becomes unreliable and ignoring data kills the sample. A proposed solution to this problem is presented below.

Let's call the normalized inverse of the scatter matrix of c fabric elements L^c as $L^{\perp c}$

$$L^{\perp c} = \frac{(L^c)^{-1}}{\mathrm{tr}\big((L^c)^{-1}\big)}, \tag{2.3}$$

where tr stands for the trace of a matrix.

Then using equation (2.3), I define a pooled scatter matrix $L^{b,c}$ as

$$L^{b,c} = \frac{n_b L^b + n_c L^{\perp c}}{n_b + n_c}, \tag{2.4}$$

where n_b and n_c are sample sizes of b- and c-structures.

Now, the β-axis can be estimated by the eigenvector of $L^{b,c}$ corresponding to the maximum eigenvalue:

$$\beta^{b,c} = \upsilon_1^{L^{b,c}}. \tag{2.5}$$

So what is the meaning of the scatter and inverse scatter matrices? It is clear that the eigenvectors of the scatter matrix define a location of a distribution of the orientation data. As a matter of fact, these eigenvectors are the maximum likelihood estimators for location parameters of a number of spherical distributions (see Mardia & Jupp, 2000). Eigenvalues of this matrix define a density of the observations around the corresponding eigenvectors. So the first eigenvector is one of the three orthogonal directions with the maximum concentration of data points around it and the third eigenvector has the least number of points in its neighborhood. Now it should be clear why the first eigenvector of the L^b matrix can be used as an estimator of β axis. The uncertainty of this estimator will increase as the first eigenvalue decreases. Besides that, the uncertainty in the direction of the second eigenvector increases as the second eigenvalue increases. Indeed, the greater it is, the higher the girdleness of the distibution is and, consequently, the less determined the estimator is. The same thing happens with the third eigenvector and eigenvalue.

Therefore the uncertainty of the direction of the first eigenvector can be decomposed into uncertainties along the directions of the second and third eigenvectors. Let's put this in the following notation:

$$\mathrm{unc}(v_1) = \begin{bmatrix} \mathrm{unc}_2(v_1) & \\ & \mathrm{unc}_3(v_1) \end{bmatrix} \tag{2.6}$$

here the subscript at unc stands for the component of the uncertainty. This is almost like a scatter matrix of two dimensional linear data, except now it is on a two dimensional surface of a sphere.

Rewriting this for the L^b matrix obtain

$$\mathrm{unc}(v_1^{L^b}) \sim \begin{bmatrix} \frac{\lambda_2}{\lambda_1} & \\ & \frac{\lambda_3}{\lambda_1} \end{bmatrix}_{L^b} \tag{2.7}$$

Now consider the L^c scatter matrix. The c-fabrics are commonly distributed along a great circle. This means that they all lay approximately in the same plane and have various directions. This also means that the concentration of the axes around the first and second eigenvectors will be approximately the same, therefore the maximum and intermediate eigenvalues will be close. The difference will increase as clustering of the data around a single direction increases. Now recall that the normal to the great circle of c-fabrics corresponds to the β-axis. Therefore it can be estimated by the minimal eigenvalue of the L^c scatter matrix. The uncertainty of this estimator will increase with the third eigenvalue increasing. In the directions of the first and second eigenvectors it will be inversely proportional to the first and second eigenvalues correspondingly. Using the notation similar to one defined in the equation (2.6) I can write

$$\mathrm{unc}^{-1}(v_3^{L^c}) \sim \begin{bmatrix} \frac{\lambda_2}{\lambda_3} & \\ & \frac{\lambda_1}{\lambda_3} \end{bmatrix}_{L^c} \tag{2.8}$$

Here unc^{-1} stands for certainty (or inverse uncertainty if you prefer).

It is quite easy to show that a first eigenvector of a matrix[2] equals the third eigenvector of its inverse matrix and vice versa. The following eigenvalue ratios are true as well:

$$\frac{\lambda_3^L}{\lambda_2^L} = \frac{\lambda_2^{L^{-1}}}{\lambda_1^{L^{-1}}}, \qquad \frac{\lambda_2^L}{\lambda_1^L} = \frac{\lambda_3^{L^{-1}}}{\lambda_2^{L^{-1}}}, \qquad \frac{\lambda_3^L}{\lambda_1^L} = \frac{\lambda_3^{L^{-1}}}{\lambda_1^{L^{-1}}}, \tag{2.9}$$

Therefore the equation (2.8) can be rewritten as

$$\text{unc}(\upsilon_3^{L^c}) \sim \begin{bmatrix} \frac{\lambda_3}{\lambda_2} & \\ & \frac{\lambda_3}{\lambda_1} \end{bmatrix}_{L^c} = \begin{bmatrix} \frac{\lambda_2}{\lambda_1} & \\ & \frac{\lambda_3}{\lambda_1} \end{bmatrix}_{L^{\perp c}} \sim \text{unc}(\upsilon_1^{L^{\perp c}}) \tag{2.10}$$

The right hand side expression is identical to the equation (2.7). Both these expressions show the variance of a β-axis estimator. The first one is for the variance of β^b and the second for the variance of β^c. Since they express the uncertainty in the same way and are using corresponding eigenvalues, the pooled estimator can be obtained by simple summation of the scatter matrices L^b and $L^{\perp c}$ like it is done in the equation (2.4). This equation also accounts for the possible difference in the sample sizes scaling the scatter matrices proportionally.

In most cases fabric data is collected over some area and the question of interest is whether any spatial trend is present or not. Below, I present a few methods which can be used to investigate spatial variability.

2.2 Assessing Spatial Trend I. Kernel Smoothing

Kernel smoothing is useful for exploratory purposes. The idea is to compute the scatter matrix (either pooled or separately for each fabric type) over a grid assigning weights to the observations according to some function of distance between the grid node

[2] Every time time you read "matrix", understand it as "positive definite symmetric real matrix"

and location of the observation (see Duda et al., 2000, Hallin et al., 2004, Bowman & Azzalini, 1997).

Let A be a matrix composed of rows of data points $\boldsymbol{a}_j$. Then, for a particular grid point $\boldsymbol{g}_i$, the weighted data matrix $\widehat{A}_i$ will consist of row vectors

$$\hat{\boldsymbol{a}}_j^i = \mathrm{k}(\boldsymbol{g}_i, \boldsymbol{s}_j)\boldsymbol{a}_j \tag{2.11}$$

where k is a kernel function and $\boldsymbol{s}_j$ is a location of the j^{th} observation.

The weighted scatter matrix will be defined analogous to equation (2.1) as

$$\widehat{L}_i^a = n^{-1}\widehat{A}_i^T\widehat{A}_i \tag{2.12}$$

This operation will produce a scatter matrix field which can be further explored in different ways. The simplest and most commonly used smoother is a properly scaled inverse distance kernel function.

This non-parametric technique can show the spatial behavior of the fabric distribution.

2.3 Assessing Spatial Trend II. Model Based Approach

It is often preferable to have some simple model which explains only a particular feature of data, omitting other features as a noise. Here I am going to introduce several models aiming to describe the spatial trend of β-axis. Also a method of fitting these models to data will be presented.

In linear data analysis one of the most widely used modeling techniques is linear regression. Unfortunately orientation data does not withstand linear transformations with the exception of rotations and identity transformations. Fortunately rotation is all we need.

Let's represent the orientation of the β-axis as a product of a spatially dependent rotation of some constant reference axis:

$$\beta_{(\boldsymbol{s})} = \mathcal{R}(\boldsymbol{r}(\boldsymbol{s}))\beta_0 \tag{2.13}$$

where $\boldsymbol{r}(\boldsymbol{s}) \in \mathbb{R}^3$ is some function of spatial location; $\mathcal{R} \in \mathrm{SO}(3)$ is a rotation operator and $\beta_0 \in S^2$ a reference axis.

There exist a number of mathematical representations of rotations (for more in-depth discussion see Altmann, 1986). Probably the most commonly used one is an orthogonal matrix. It has useful algebraic properties and is convenient for computation. These matrices are members of SO(3) space.

Another representation of rotations is a pseudo-vector. The only difference from a regular vector is that the sign of a pseudo-vector does not change under improper rotations. In a representation of rotation, the direction of the pseudo-vector is treated as the axis of rotation and its length is the sine of the rotation angle. Pseudo-vectors, as rotations, do not possess nice properties. For example there is no simple operation which would combine two consecutive rotations. Therefore pseudo-vectors are rarely used for this purpose. However they do have one really important property for this study — they are members of $\mathbb{R}^3$. This means that standard statistical procedures can be applied to model rotations.

As it was mentioned above, $\mathcal{R}$ range is SO(3), i.e. values of this function are 3×3 orthogonal matrices. As its domain we are free to choose any representation of rotation suitable for linear modeling. From the previous paragraph it follows that a pseudo-vector is a good candidate for that. One of its negative features follows from the property $\|\boldsymbol{r}\| = \sin\theta$. This means that number of revolutions associated with this representation is not limited. Therefore there are multiple representations of the same model[3], which

[3] For axes, rotations $n\pi, n \in \mathbb{Z}$ are indistinguishable

is undesirable since it may lead to problems with optimization (which will be described later in this chapter). On the other hand, this representation allows for more than a single revolution in the limits of a single model. However, the importance of this kind of model for geology is doubtful.

To resolve the problem of multiple rotations I will replace sine with tangent obtaining

$$\boldsymbol{r} = \boldsymbol{n} \tan\theta, \tag{2.14}$$

where $\boldsymbol{n}$ is a unit vector. The transformation $\|\boldsymbol{r}\| = \tan\theta$ maps $\|\boldsymbol{r}\| \in \mathbb{R}$ to $\theta \in (-\pi/2, \pi/2)$. This representation is suitable for moderate (say less than $2\pi/3$) angles of rotation inside a model. This restriction seems to be reasonable for most problems. Otherwise the standard pseudo-vector interpretation must be used.

Using representation (2.14) and an expression for an orthogonal matrix of a rotation ($\theta\boldsymbol{n}$) given by Altmann (1986, chap. 3.3), a SO(3)-valued function $\mathcal{R}$ from equation (2.13) can be written as

$$\mathcal{R}(\boldsymbol{r} : \boldsymbol{r} = \boldsymbol{n}\tan\theta) = \begin{pmatrix} 1 - 2(n_2^2 + n_3^2)\sin^2\frac{1}{2}\theta & -n_3\sin\theta + 2n_1n_2\sin^2\frac{1}{2}\theta & n_2\sin\theta + 2n_1n_3\sin^2\frac{1}{2}\theta \\ n_3\sin\theta + 2n_1n_2\sin^2\frac{1}{2}\theta & 1 - 2(n_1^2 + n_3^2)\sin^2\frac{1}{2}\theta & -n_1\sin\theta + 2n_2n_3\sin^2\frac{1}{2}\theta \\ -n_2\sin\theta + 2n_1n_3\sin^2\frac{1}{2}\theta & n_1\sin\theta + 2n_2n_3\sin^2\frac{1}{2}\theta & 1 - 2(n_1^2 + n_2^2)\sin^2\frac{1}{2}\theta \end{pmatrix} \tag{2.15}$$

2.3.1 "Full" Model

Consider a linear model

$$\boldsymbol{R} = \boldsymbol{S}\Psi, \tag{2.16}$$

where $\boldsymbol{R}$ is matrix of rotations represented according to equation (2.14), $\boldsymbol{S}$ is a matrix of spatial coordinates with the first column added to account for an intercept and Ψ is the model parameter matrix.

$$\boldsymbol{R} = \begin{pmatrix} r_{11} & \cdots & r_{1p} \\ \vdots & \ddots & \vdots \\ r_{n1} & \cdots & r_{np} \end{pmatrix} \qquad \boldsymbol{S} = \begin{pmatrix} 1 & s_{11} & \cdots & s_{1q} \\ \vdots & \vdots & \ddots & \vdots \\ 1 & s_{n1} & \cdots & s_{nq} \end{pmatrix} \qquad \Psi = \begin{pmatrix} \psi_{01} & \cdots & \psi_{0p} \\ \psi_{11} & \cdots & \psi_{1p} \\ \vdots & \ddots & \vdots \\ \psi_{q1} & \cdots & \psi_{qp} \end{pmatrix}$$

In vector form the equation (2.16) can be written as

$$\begin{aligned} \boldsymbol{r}(\boldsymbol{s}_k) = \Psi^T \boldsymbol{s}_k = \\ = \begin{pmatrix} \psi_{10} + \psi_{11} s_{k1} + \cdots + \psi_{1q} s_{kq} \\ \vdots \\ \psi_{p0} + \psi_{p1} s_{k1} + \cdots + \psi_{pq} s_{kq} \end{pmatrix}, \end{aligned} \tag{2.17}$$

where $\boldsymbol{s}_k$ is a k^{th} row of the $\boldsymbol{S}$ matrix written as a column vector, i.e. $\boldsymbol{s}_k = (1, s_{k1}, \ldots, s_{kq})^T$.

This model defines a linear field of $\mathbb{R}^p$ vectors in $\mathbb{R}^q$ space. In structural geology $p = 3$ almost always, but geographical space may be considered either two or three dimensional. Throughout this paper $q = 2$.

Now, from equations (2.13) and (2.17) obtain

$$\beta_{(\boldsymbol{s}_k)} = \mathcal{R}(\Psi^T \boldsymbol{s}_k)\beta_0. \tag{2.18}$$

This determines a model for the β-axis in a structural frame. As I mentioned above, the γ-axis (corresponding to c-fabrics) is assumed to be normal to β:

$$\gamma^T_{(\boldsymbol{s}_k)} \beta_{(\boldsymbol{s}_k)} = 0. \tag{2.19}$$

This is the only restriction on the γ-axis in this model. Its rotations around β are not considered. The main purpose of the current section is to model β-axis behavior and the γ-axis is introduced only to allow c-fabrics related to it to contribute some information.

Now, once the model is formulated, a technique to find its optimal parameters must be developed. Traditionally this is done by minimizing total deviation of data from a model. A natural way to express the distance on a sphere is the angle between $\mathbb{R}^3$ vectors corresponding to the $S^{1,3}$ data (embedding approach).

Providing a model for the β-axis and data on b- and c-fabrics, the objective function can be defined as follows

$$\epsilon(\Psi, \beta_0) = \sum_{i=1}^{n_b} \theta\big(\boldsymbol{b}_i, \beta_{(\boldsymbol{s}_i)}\big) + \sum_{i=1}^{n_c} \Big(\pi/2 - \theta\big(\boldsymbol{c}_i, \beta_{(\boldsymbol{s}_i)}\big)\Big) \tag{2.20}$$

where $\beta_{(s_i)}$ is determined according to the equation (2.18), n_b and n_c are the sizes of b- and c-fabric samples respectively. Function θ is a suitable measure of an angle between two orientations. In the case of direction it is defined by equation (1.2) and for axes — by equation (1.3).

The first summation in equation (2.20) reflects the deviation of measurements of b-structures from the modeled β. The second summation corresponds to the deviation of c-fabrics from the normality condition in equation (2.19). Rewriting equations (2.20) and (2.18) together and minimizing overall error, the estimator for model parameters is obtained

$$\begin{aligned}(\Psi, \beta_0)^{b,c} = \arg\min_{\Psi,\beta_0} \Big(\sum_{i=1}^{n_b} \theta\big(\boldsymbol{b}_i, \mathcal{R}(\Psi^T \boldsymbol{s}_k)\beta_0\big) + \\ + \frac{n_c \pi}{2} - \sum_{i=1}^{n_c} \theta\big(\boldsymbol{c}_i, \mathcal{R}(\Psi^T \boldsymbol{s}_k)\beta_0\big)\Big).\end{aligned} \tag{2.21}$$

Assume the orientations to be $G^{1,3}$ axes in $\mathbb{R}^2$ geographical space.[4] This model now contains a total of 11 parameters: Ψ 3×3 matrix contributes nine and $\beta_0 \in S^2$ gives two. However, β_0 actually can be absorbed by Ψ and therefore it can be chosen arbitrarily. This reduces dimensionality of the parameter space to $\mathbb{R}^9$.

[4] This assumption will stay till the end of this paper.

The final solution then becomes

$$(\Psi)^{b,c} = \arg\min_{\Psi}\Big(\sum_{i=1}^{n_b}\theta\big(\boldsymbol{b}_i, \mathcal{R}(\Psi^T\boldsymbol{s}_k)\beta_0\big) + \\ + \frac{n_c\pi}{2} - \sum_{i=1}^{n_c}\theta\big(\boldsymbol{c}_i, \mathcal{R}(\Psi^T\boldsymbol{s}_k)\beta_0\big)\Big)\Big|_{\beta_0} \tag{2.22}$$

It should be mentioned that while choosing the reference axis β_0 one should remember about limitations on the rotation angle created by representation (2.14). Therefore the $\beta^{b,c}$ point estimator defined by equation (2.5) should be taken as a reference axis.

2.3.2 Small Circle Model

The model defined by equation (2.18) allows significant flexibility regarding the trend of the β-axis. Sometimes it may be desirable to have a simpler but more restrictive model. First, it may be hard to assign any geological meaning to the "full" model. Besides that, the more parameters in a model, the bigger the sample size needed.

One obvious simplification is to hold the axis of rotation fixed. This leads to the following decomposition of the Ψ matrix:

$$\Psi = \begin{pmatrix} \psi_0 \\ \vdots \\ \psi_q \end{pmatrix} \begin{pmatrix} r_{01} & \cdots & r_{0p} \end{pmatrix} = \psi\boldsymbol{r}_0^T. \tag{2.23}$$

Using equations (2.13) and (2.17) obtain

$$\beta_{(\boldsymbol{s})} = \mathcal{R}(\boldsymbol{r}_0\psi^T\boldsymbol{s})\beta_0 \tag{2.24}$$

The model restricts the β orientation to a small circle, which gives rise to the name.

In the case of $p = 3$ and $q = 2$ this model contains a total of seven parameters (using the $2(p-1)+(q+1)$ rule). Unlike the "full" model, β_0 cannot be absorbed by ψ completely. However given $\boldsymbol{r}_0$, the β_0 orientation needs to be defined only by an angle

which it makes with $\boldsymbol{r}_0$. The rest can be accounted by ψ vector. Therefore, the actual number of parameters in this model is six.

Estimation of the model parameters is analogous to equation (2.22)

$$(\psi, \boldsymbol{r}_0, \theta_0)^{b,c} = \underset{\psi,\boldsymbol{r}_0,\theta_0}{\arg\min}\Big(\sum_{i=1}^{n_b} \theta\big(\boldsymbol{b}_i, \mathcal{R}(\boldsymbol{r}_0\psi^T\boldsymbol{s})\beta_0\big) + \\ + \frac{n_c\pi}{2} - \sum_{i=1}^{n_c} \theta\big(\boldsymbol{c}_i, \mathcal{R}(\boldsymbol{r}_0\psi^T\boldsymbol{s})\beta_0\big)\Big)\Big|_{\beta_0^T\boldsymbol{r}_0=\cos\theta_0} \tag{2.25}$$

Again, as in the previous model, β_0 should be chosen close to the average β (see remarks below the equation (2.22)).

2.3.3 Great Circle Model

A further simplification is to constrain angle between β_0 and $\boldsymbol{r}_0$ to $\pi/2$. This will bring all β onto the same great circle. Hence the name.

Solution for the parameters of this model is derived from equation (2.25)

$$(\psi, \boldsymbol{r}_0)^{b,c} = \underset{\psi,\boldsymbol{r}_0}{\arg\min}\Big(\sum_{i=1}^{n_b} \theta\big(\boldsymbol{b}_i, \mathcal{R}(\boldsymbol{r}_0\psi^T\boldsymbol{s})\beta_0\big) + \\ + \frac{n_c\pi}{2} - \sum_{i=1}^{n_c} \theta\big(\boldsymbol{c}_i, \mathcal{R}(\boldsymbol{r}_0\psi^T\boldsymbol{s})\beta_0\big)\Big)\Big|_{\beta_0^T\boldsymbol{r}_0=0} \tag{2.26}$$

It further reduces number of parameters to five.

2.3.4 "Null" Model

The last reduction of this model is to remove the spatial component completely, i.e. to put

$$\Psi = \begin{pmatrix} 0 & \cdots & 0 \\ \vdots & \ddots & \vdots \\ 0 & \cdots & 0 \end{pmatrix} \tag{2.27}$$

in equation (2.17). According to the equation (2.15) this leads to

$$\mathcal{R} = \begin{pmatrix} 1 & 0 & 0 \\ 0 & 1 & 0 \\ 0 & 0 & 1 \end{pmatrix} \tag{2.28}$$

everywhere. In this case solution for the parameters becomes simply

$$\begin{aligned} (\beta_0)^{b,c} = \arg\min_{\beta_0} \Big(& \sum_{i=1}^{n_b} \theta\big(\boldsymbol{b}_i, \beta_0\big) + \\ & + \frac{n_c \pi}{2} - \sum_{i=1}^{n_c} \theta\big(\boldsymbol{c}_i, \beta_0\big) \Big) \end{aligned} \tag{2.29}$$

This estimator is similar to one defined by equation (2.5).

2.4 Spatial Autocorellation

All of the estimators in section 2.3 implicitly assume independence between observations in each group. However, spatial data is rarely independent, but tend to display some degree of correlation, which is usually a function of geographical distance between points. This feature of spatial data leads to a reduction of total weight that should be assigned to observations in a closely spaced cluster because they are correlated and, so to speak, share the same bits of information about population from which the sample is drawn.

So the problem to solve when dealing with spatial data is to estimate a degree of autocorrelation and use it to assign appropriate weights to the observations. This task requires a correlation model that can be fitted. To investigate properties of a spatial process, geostatistics operates with a set of so called stationary random functions (for more details refer to Schabenberger & Gotway, 2005, Ripley, 2004, Haining, 2003, Houlding, 2000, Chilès & Delfiner, 1999, Rivoirard, 1994, Cressie, 1993, Griffith, 1988, Young, 1987b, Upton & Fingleton, 1985).

An often used intrinsic stationary model assumes

$$E\big(Z(\boldsymbol{s}+\boldsymbol{h})-Z(\boldsymbol{s})\big)=0 \tag{2.30a}$$

$$E^2\big(Z(\boldsymbol{s}+\boldsymbol{h})-Z(\boldsymbol{s})\big)=2\gamma(\boldsymbol{h}), \tag{2.30b}$$

where $\{Z(\boldsymbol{s}) : \boldsymbol{s} \in D \subset \mathbb{R}^q\}$ is a q-dimensional spatial random function defined over a domain D, $\boldsymbol{s}$ is a spatial index and $\boldsymbol{h} \in \mathbb{R}^q$ is a separation vector; E stands for expectation and E^2 is variance. Quantity γ is called *semivariogram*. It is the parameter of autocorrelation for this model.

From equation (2.30a) it follows that in order to use this model, data must be first detrended. However to estimate the trend of data one has to know the autocorrelation structure. To resolve this problem, trend is usually estimated neglecting the autocorrelation aspect of data. Then, using residuals, which hopefully will have an approximately constant mean, the variogram is estimated and used to fit the trend again but armed with the modeled autocorellation structure this time. To obtain better results this procedure can be repeated recursively.

Spatial analysis of orientation data currently is not very well developed. Young (1987a,b) and later van den Boogaart & Schaeben (2002a,b) used the embedding approach to map orientation data to a linear space, then did an analysis using linear geostatistics and then mapped the results back to the manifold. Unfortunately, there is no such bijective transformation between the linear space and the manifold. Therefore the trend in embedding space does not generally belong to the manifold.

CHAPTER 3

ANALYSIS OF THE KUKAS LAKE STRUCTURE

3.1 Data description

3.1.1 Geological settings of the Kukas lake structure

Data used in this research was collected during structural mapping of the Eastern part of the Kukas lake area (North Karelia, Russia) shown on figure 3.1. This region is on the Baltic shield and is situated on the border between two Archean cratons: Belomorskii on the North and Karelskii on the South. Therefore the Kukas lake structure is commonly interpreted as an orogenic belt produced by collision of those cratons. According to some other interpretations the whole Belomorskii block with the Kukas lake structure is an orogenic belt between the Karelskii and Kolskii cratons. The later is situated North of the Belomorskii block.

The Kukas lake structure is composed of Early Proterozoic volcanic and sedimentary formations metamorphosed to amphibolite facies during Svecofenian time (2–1.8 Ga, which approximately corresponds to the Orosirian). These rocks are conformably underlaid by Archean amphibolites and gneisses referred to as Lopii strata. The Karelskii and Belomorskii blocks are mostly composed of Archean gneisses and amphibolites.

Besides other problems, the curvature of the structure has attracted some interest. There are two contradicting opinions on this. One interprets this curvature as a result of curvature of one of cratons participating in the collision. In this case the flanks of the structure are expected to be deformed in a transpressional regime — dextral to the East and sinistral to the West. Another interpretation claims that this curvature is not related to this orogeny, but caused by some later event.

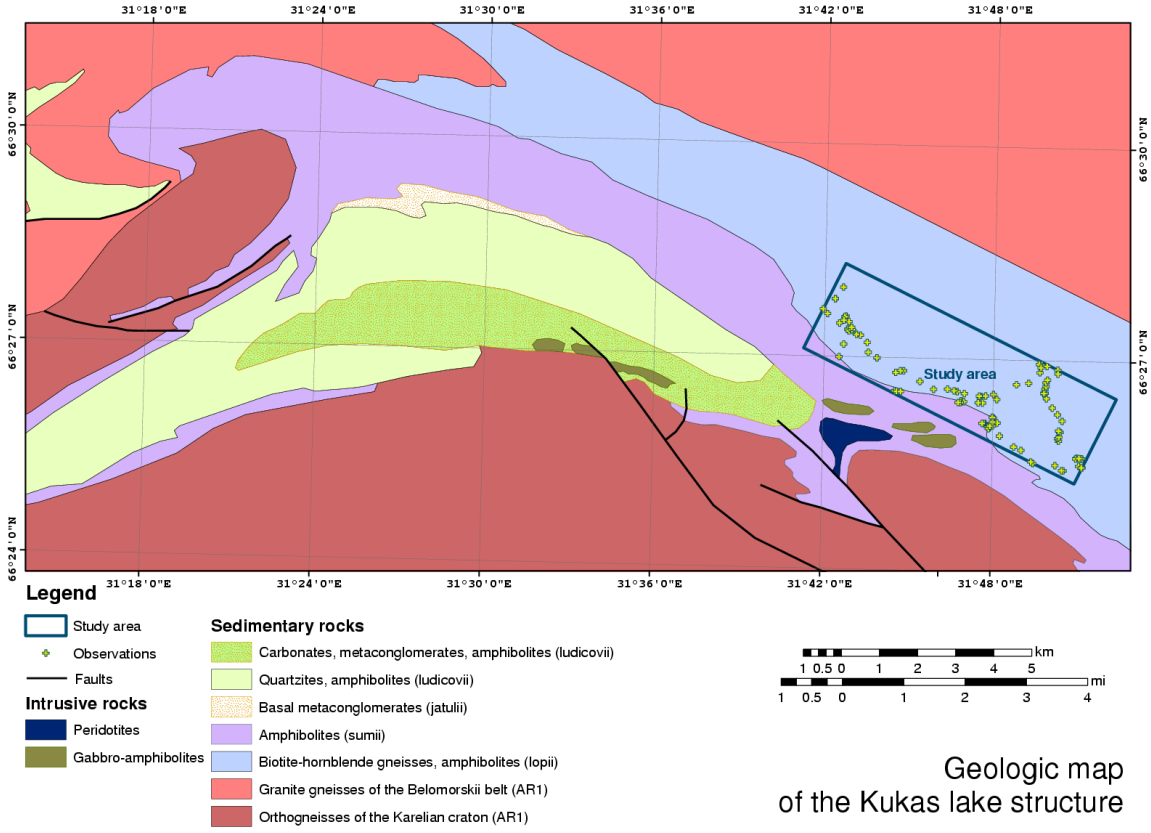

Figure 3.1 Geological map of the Kukas lake structure (after Somin & Travin, 2002) and the region of study.

In the first case, the metamorphic fabrics should reflect a transpressive zone, which were modeled quite extensively (e.g. Robin & Cruden, 1994).

In the other case all the structure should be rotated, possibly with little evidence of strain associated with it. Presumably there was no metamorphism associated with this rotation.

Some transpressional conditions could occur even without the presence of a curved craton. However in this case the shear sense on both flanks of the structure should be the same.

3.1.2 Fabric observations

Collected during the 2002 field season the observations include measurements of schistosity and bedding planes, intersectional biotite lineation, fold axes and axes of winged inclusions. There is a total of 349 measurements of different kinds collected over the area of approximately 20 km^2.

Schistosity is primarily related to the parallel orientation of biotite and is parallel to the bedding when it is observed. Travin (1992) showed that the lineation is caused by a girdle distribution of biotite. Such interpretation implies the exclusive occurrence of either schistosity or lineation. Indeed, it was noticed that the schistosity is more common at the East part of the studied area, while the lineation becomes more prominent towards West. However, both textures were sporadically observed together. This can be explained by an incomplete girdle distribution of biotite. The maximum eigenvector of the biotite orientation scatter matrix appeared as schistosity and the minimum value eigenvector as lineation. Therefore both, lineation and foliation in this area are probably just different aspects of the same rock texture that is biotite preferred orientation.

Schistosity, bedding, lineation and fold axes are the four major fabric elements which will be used in this study. As it was mentioned above, schistosity is parallel to bedding (c-fabrics) and lineation is parallel to fold axes (b-fabrics). Also, normals to the c-fabrics are perpendicular to the b-fabrics.

The goal of this chapter is to verify these observations statistically and to discover possible spatial trends of the orientations.

3.2 Exploratory Analysis

Before fitting the models to the observations it is helpful to get some idea about what this data look like. This section highlights a few aspects of the Kukas lake sample using some visual techniques for the exploratory analysis of the orientation data.

All of the plots to be presented make use of the Lambert (or Schmidt) equal-area azimuthal projection. This projection is a bijective transformation from a hemisphere in $\mathbb{R}^3$ to a disk in $\mathbb{R}^2$. It is given by

$$\begin{pmatrix} x_1 \\ x_2 \end{pmatrix} = \sqrt{2} \sin \frac{\phi}{2} \begin{pmatrix} \cos\theta \\ \sin\theta \end{pmatrix}, \tag{3.1}$$

where θ corresponds to a trend of an orientation, ϕ is its plunge and (x_1, x_2) are the coordinates of the projected orientation. This transformation is standard for structural geology. Another convention is to use the lower hemisphere to project axes. It is reflected by a requirement $\phi \in (0, \pi/2)$.

Figure 3.2 shows the overall scatter of different observations of the fabrics. Great circles shown on the picture correspond to eigenvectors of the scatter matrix L^c of c-fabrics. The crossed circle is $v_1^{L^b}$, an eigenvector of the maximum eigenvalue of the b-fabrics scatter matrix (see page 9 for the notation). This axis is an estimator β^b of the β-axis of the structural frame. At the same time, eigenvector $v_3^{L^c}$ of the scatter matrix L^c can be considered an estimator of the β-axis as well.

Estimates of β from lineation and foliation data are

$$\beta^b = (303, 27) \qquad \text{and} \qquad \beta^c = (310, 16)$$

respectively (measurements are given in Euler angles and degrees). The angle between the estimators is 13°.

Is this difference significant? Mathematically sound methods of statistical inference for this kind of problem are still to be developed. For now I will use the following qualitative procedure.

First, for both groups of observations, some number of bootstrap resamples from the original data are generated. Then, for each of the bootstrapped samples and for each group, compute the estimate of the β axis. Finally, plot both groups of the estimates on a stereonet. Overlapping clusters will suggest no significant difference between β^b and β^c, while clearly separated clusters will indicate the opposite.

Figure 3.3 shows the scatter of 100 bootstrapped estimates β^b and β^c. The clusters are clearly separated, therefore the average direction of the b-fabrics can not be considered normal to the best-fit girdle of the c-fabrics as was assumed.

There are two possible causes of this problem. At first, it may just be that the assumption of normality is wrong, although this explanation might not be very satisfying for a structural geologist. Another reason for the apparent non-normality may be presence of a spatial trend, which was not considered by those estimators.

To check this possibility I will use the kernel smoothing method explained in section 2.2.

Figure 3.4 shows the result of smoothing. It was obtained in the following way. First a six by two spatial grid was generated. Then at each point of the grid a vector of weights was computed using a Gaussian radial basis kernel function (GRBF), which is defined as

$$\mathrm{k}(\boldsymbol{g}_i, \boldsymbol{s}_j) = \exp(-\sigma \|\boldsymbol{s}_i - \boldsymbol{s}_j\|^2), \tag{3.2}$$

where σ is a parameter of the function which controls the smoothness and $\boldsymbol{g}_i$ and $\boldsymbol{s}_j$ are points in space. In this case the first point was a grid node and the second — a location of an observation.

Table 3.1 Comparison of the regression models

	Model	Opt. Time (sec)	Mean Error (deg)	Error Ratio
1	Full	28.2	9.1	0.75
2	Small Circle	24.1	9.1	0.75
3	Great Circle	13.0	9.4	0.77
4	No Rotation	0.3	12.2	1.00

Then the b- and c- fabric observations was weighted as

$$\hat{\boldsymbol{b}}_j^i = \mathrm{k}(\boldsymbol{g}_i, \boldsymbol{s}_j)\boldsymbol{b}_j \tag{3.3}$$

$$\hat{\boldsymbol{c}}_j^i = \mathrm{k}(\boldsymbol{g}_i, \boldsymbol{s}_j)\boldsymbol{c}_j. \tag{3.4}$$

These points are shown on the figure 3.4 as dots of varying intensity, which reflects their corresponding weight.

After the observations were assigned weights, scatter matrices $\left(\hat{L}^b\right)^i$ and $\left(\hat{L}^c\right)^i$ were computed at each node according to equation (2.1) and substituting A with $\hat{\boldsymbol{B}}^i$ and $\hat{\boldsymbol{C}}^i$ correspondingly. Finally using equation (2.4), the weighted pooled matrix was computed for each node. Its eigenvectors are shown on the picture 3.4 as a great circles of blue color.

The presence of some trend seems obvious. Now it would be nice to somehow quantify this trend. This is the goal of the following section.

3.3 Model Fitting

The four models discussed in section 2.3 will be fitted to the data.

Table 3.1 shows the run time for the optimization of each model on a hyper-threaded 3 GHz Intel® Pentium® 4 computer, the average deviation of the observations from the model and the ratio of this error to the error of the minimal model.

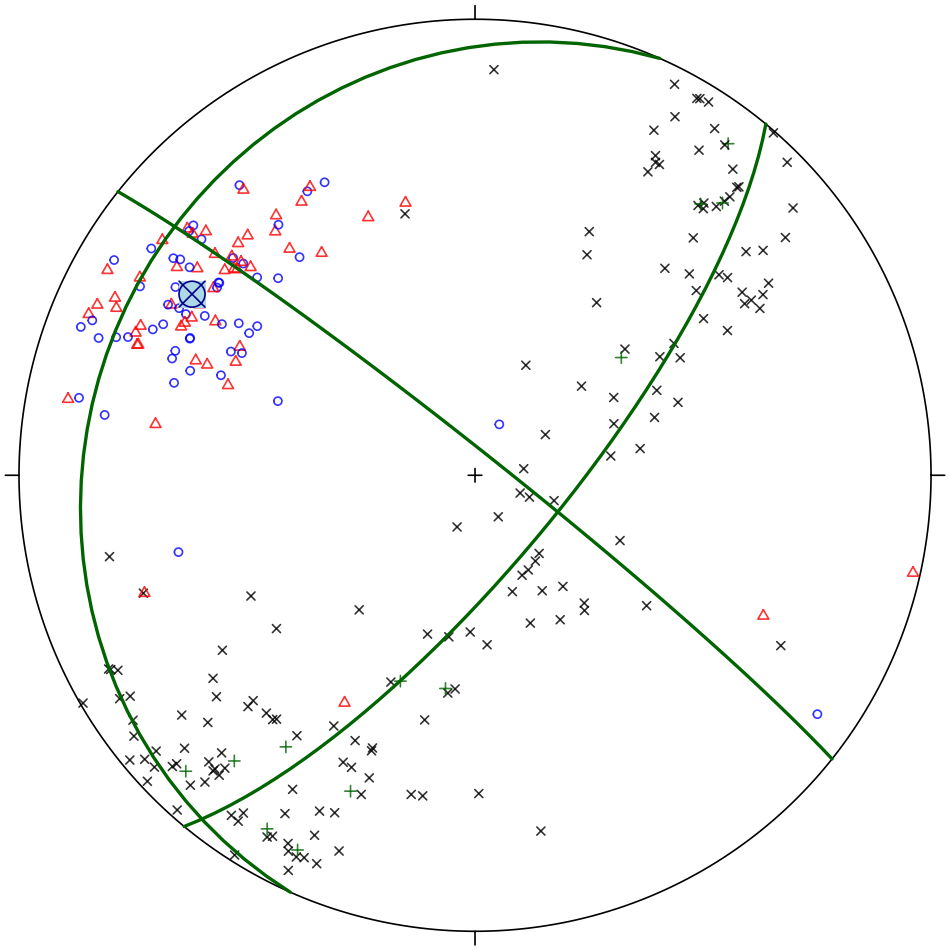

Figure 3.2 Lower hemisphere Lambert projection of fabric data collected at the study area. Dark green crosses show bedding planes, black crosses — schistosity, red triangles — lineation and blue circles — fold axes. The great circles show eigenvectors of the scatter matrix of schistosity and bedding orientations. The crossed circle is the maximum value eigenvector of the lineation and fold axes scatter matrix.

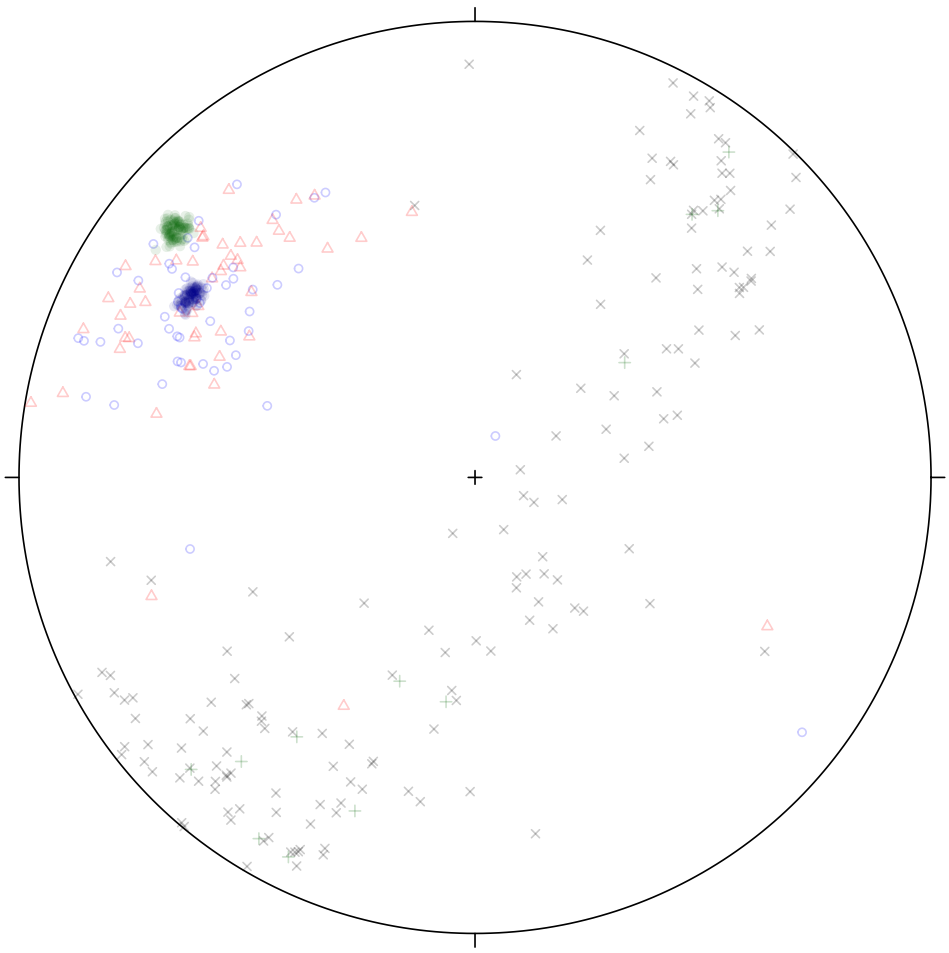

Figure 3.3 Bootstrapped estimates β^b (shown in darkblue) and β^c (darkgreen).

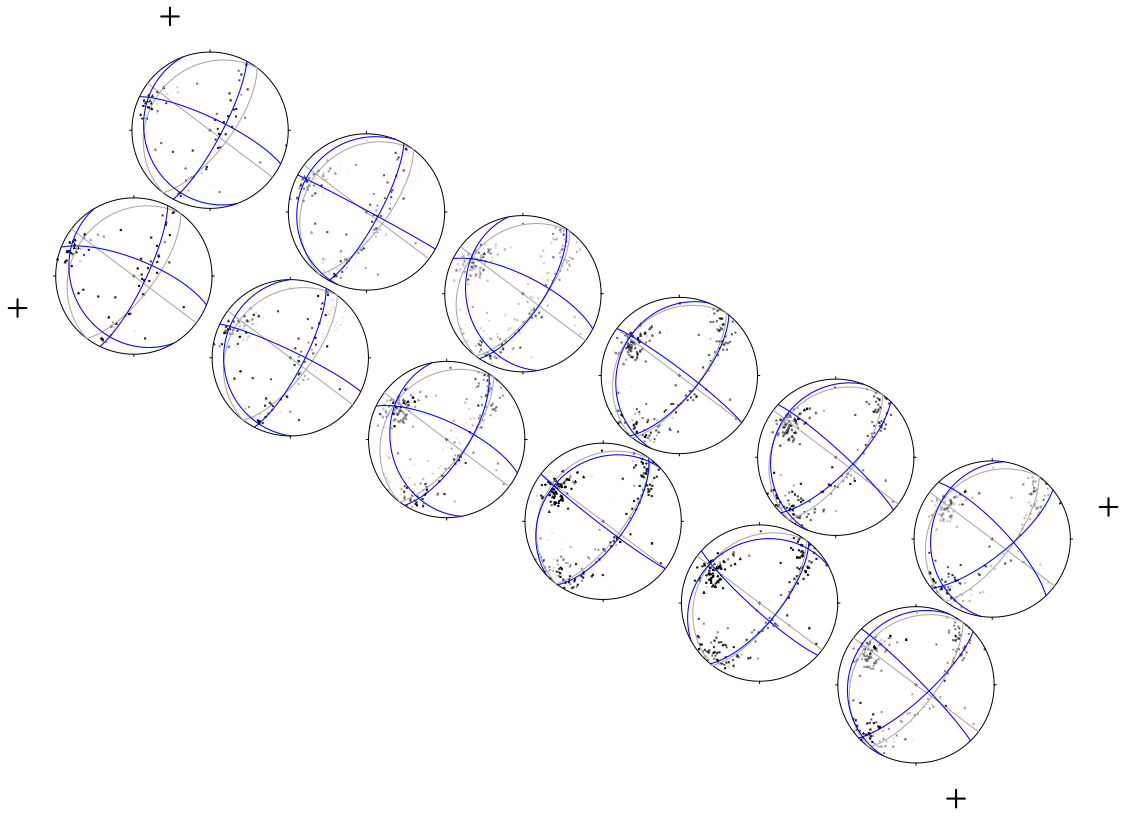

Figure 3.4 Smoothed trend over the area. Each stereonet is centered at a grid node. The intensity of points correspond to their weights. Grey colored great circles are eigenvectors of the unweighted pooled estimator $L^{b,c}$. Blue great circles correspond to the weighted pooled estimator.

From these numbers it can be seen that the resulting error of the "full" and the small circle models is almost the same. The error of the great circle model increases slightly. The error of the "null" model increases even further. That's a good thing: the smaller the model the farther the residuals. Since the "full" model in terms of the mean error is not any better than the small circle model, and it is of no special interest for structural geology, it is natural to disregard the "full" model for this dataset. However I am going to keep analyzing it just for completeness of the discussion.

The small circle model has somewhat better performance than the simpler models. So it might be the model of choice. However, with no inference procedure, it is hard to tell how significant the mean error differences are.

Now let's look at the fitted trends. Figure 3.5 shows predictions for the β axis by the "full", small circle and the great circle models. The estimators were computed at the same grid locations that were used to evaluate the smoothed trend shown in figure 3.4. Moreover, the smoothed version of the trend is reproduced together with the modeled trend for comparison. The eigenvectors of the pooled scatter matrix are shown as well.

It can be seen that all three trends are quite similar. However the rotation by the great circle model is more pronounced towards East compared to the other models.

3.3.1 Summary of the "Full" Model

The parameter matrix Ψ of the "full" model and the reference axis β_0 are

$$\Psi = \begin{pmatrix} 1.88 & -2.22 & -0.55 \\ -2.45 & 2.61 & 0.64 \\ -0.43 & 0.26 & 1.47 \end{pmatrix}, \qquad \beta_0 = \begin{pmatrix} 0.56 \\ -0.75 \\ 0.35 \end{pmatrix}.$$

The reference axis β_0 was actually chosen arbitrarily. For the reasons explained on the page 19, it was set to be equal to the pooled estimator $\beta^{b,c}$.

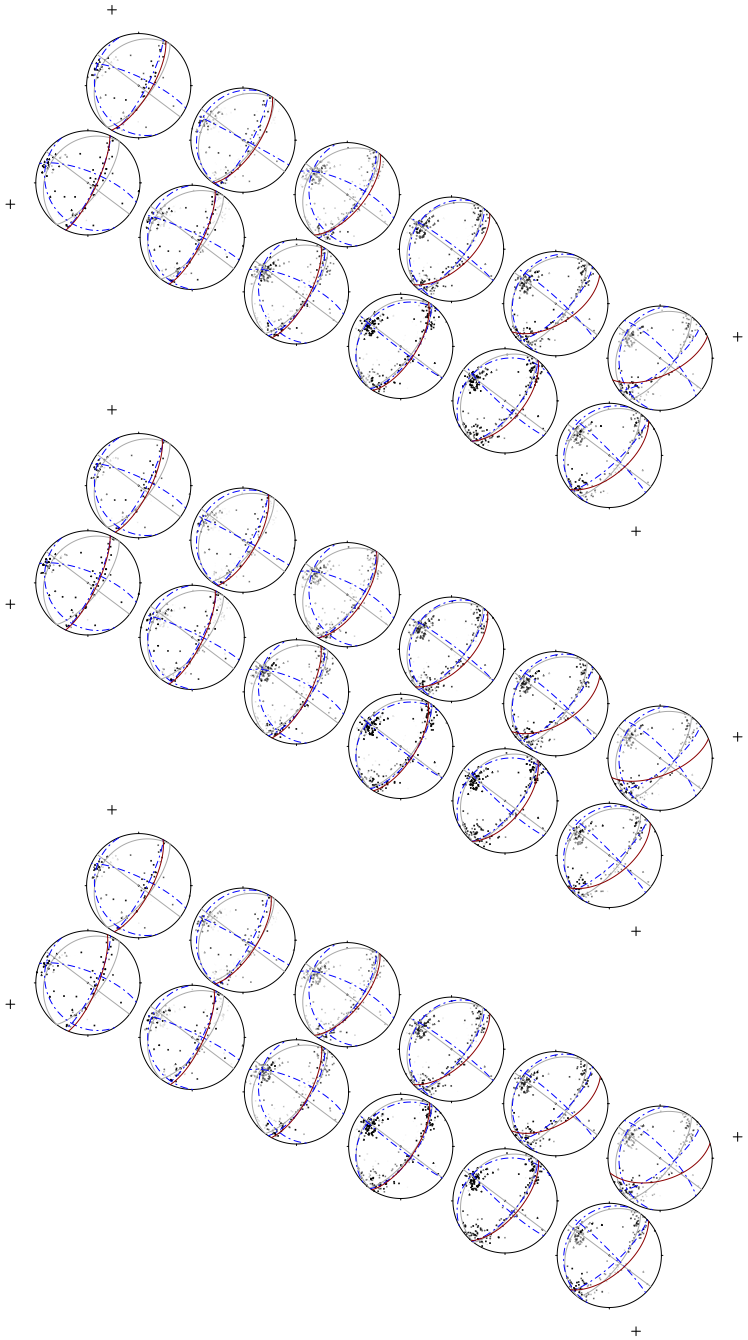

Figure 3.5 Trends (dark red) of the "full" (at the top), small circle (middle) and the great circle (bottom) models. The blue dashed lines show the kernel smoothed trend and the grey lines correspond to the eigenvectors of the pooled scatter matrix.

3.3.2 Summary of the Small Circle Model

The small circle model is parameterized by an axis of rotation r_0, reference axis β_0 and a parameter vector ψ, which actually defines a linear model for tangent of the rotation angle ($\tan\theta = \psi^T \boldsymbol{s}$, $\boldsymbol{s} = (1, s_1, s_2)$ is a space coordinate).

$$\psi = \begin{pmatrix} -4.83 \\ 5.41 \\ 2.98 \end{pmatrix}, \qquad \beta_0 = \begin{pmatrix} 0.67 \\ -0.53 \\ 0.53 \end{pmatrix}, \qquad r_0 = \begin{pmatrix} -0.78 \\ 0.62 \\ -0.06 \end{pmatrix}.$$

The angle between the r_0 and β_0 is approximately 28°.

The $\tan\theta$ model is a linear scalar field. Therefore it can be characterized by a constant gradient

$$\begin{aligned} \nabla \psi^T \boldsymbol{s} &= \left(\frac{\partial}{\partial s_1} \psi^T \boldsymbol{s}, \frac{\partial}{\partial s_2} \psi^T \boldsymbol{s} \right) = \\ &= (\psi_1, \psi_2) \end{aligned} \tag{3.5}$$

The direction of the gradient vector computed according to equation (3.5) is 61°. A normal to this direction will give a direction of no change in prediction of β.

3.3.3 Summary of the Great Circle Model

The great circle model parameterization is almost identical to the small circle model with the exception of the angle between r_0 and β_0 which is restricted to $\pi/2$.

Optimized values for the parameters are given below.

$$\psi = \begin{pmatrix} -3.79 \\ 3.39 \\ 2.41 \end{pmatrix}, \qquad \beta_0 = \begin{pmatrix} 0.81 \\ -0.01 \\ 0.59 \end{pmatrix}, \qquad r_0 = \begin{pmatrix} -0.59 \\ 0.01 \\ 0.81 \end{pmatrix}.$$

The direction of the gradient vector computed using the equation (3.5) is 55°.

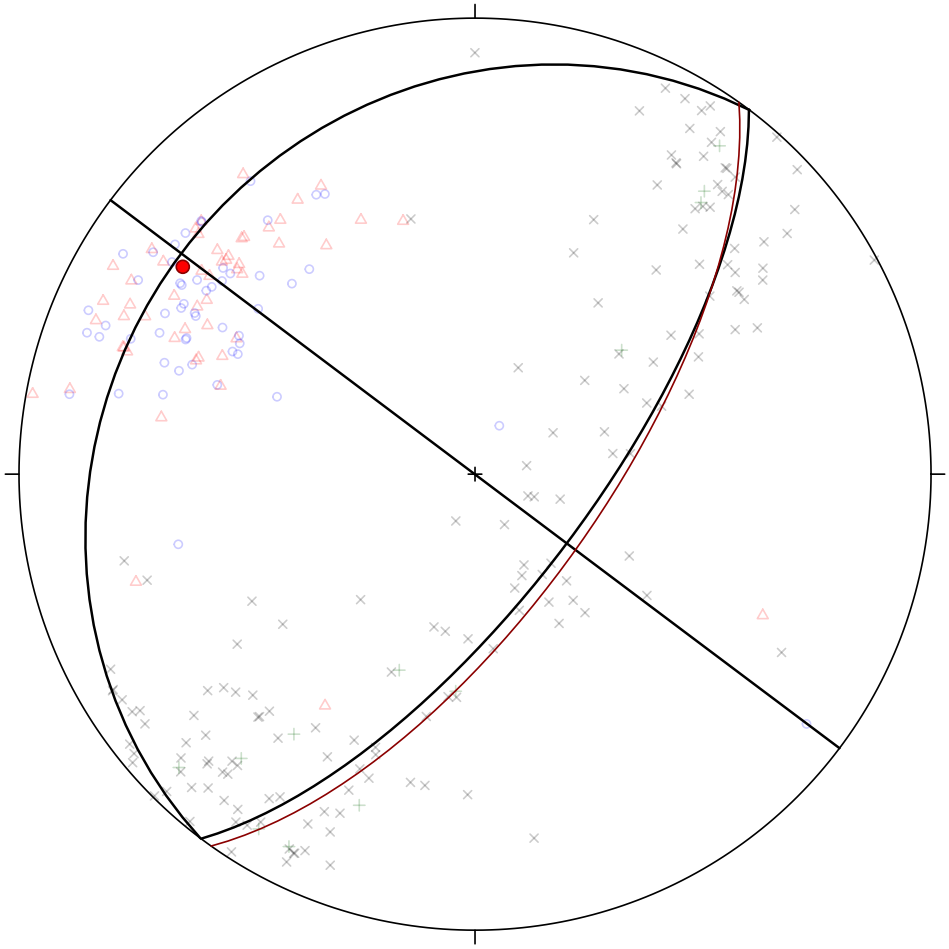

Figure 3.6 The "null" model estimate of the β_0 axis (dark red) and the pooled estimate (black).

3.3.4 Summary of the "Null" Model

The "null" model differs from the others by the absence of any trend parameters. As a matter of fact, it is analogous to the pooled estimator $\beta^{b,c}$ (equation (2.5)). It does the same job of estimating β from b and c structures using a different approach.

$$\beta_0 = \begin{pmatrix} 0.81 \\ -0.01 \\ 0.59 \end{pmatrix}.$$

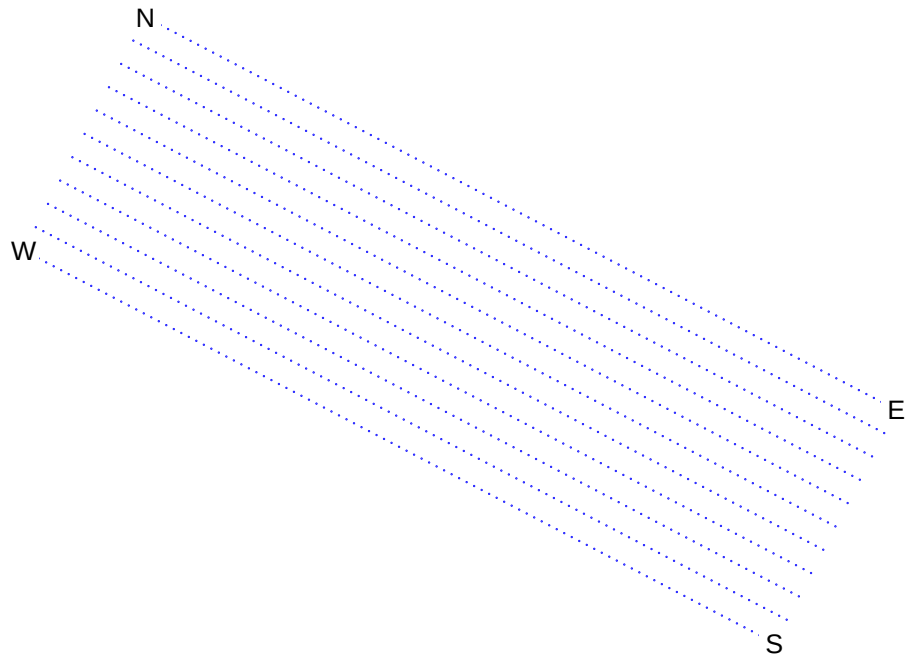

Figure 3.7 Index grid used in figures 3.8 through 3.10.

Figure 3.6 shows the β_0 estimate of the β axis (in dark red) and its relation to the pooled estimate $\beta^{b,c}$ (grey). The angle between these two is only 2°.

To better show the differences in the trends I use the following technique. Figure 3.7 shows the study area and a dense grid of locations at which the predictions by different models are computed. Corners of the area are marked with letters corresponding to their geographical orientation.

Figures 3.8 through 3.10 show these predictions for the "full", small circle and the great circle models. It is clear that all the predictions of the small circle model lay on the

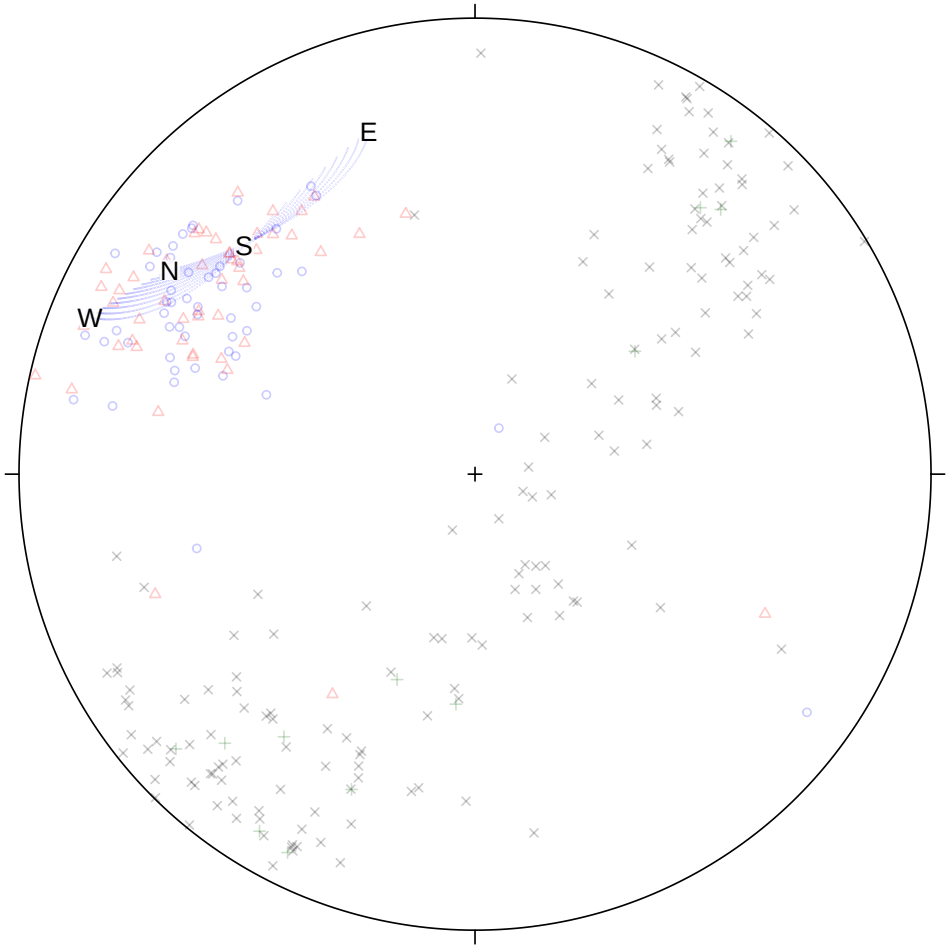

Figure 3.8 Stacked trend of the “full” model.

same small circle (as they should), and the great circle model predictions make a great circle. The images of trends for the “full” model and for the small circle model are very similar.

3.4 Residual analysis

Now, when the models are fitted and the trends observed it is time to check whether the model assumptions were correct. This is usually done by observing residuals.

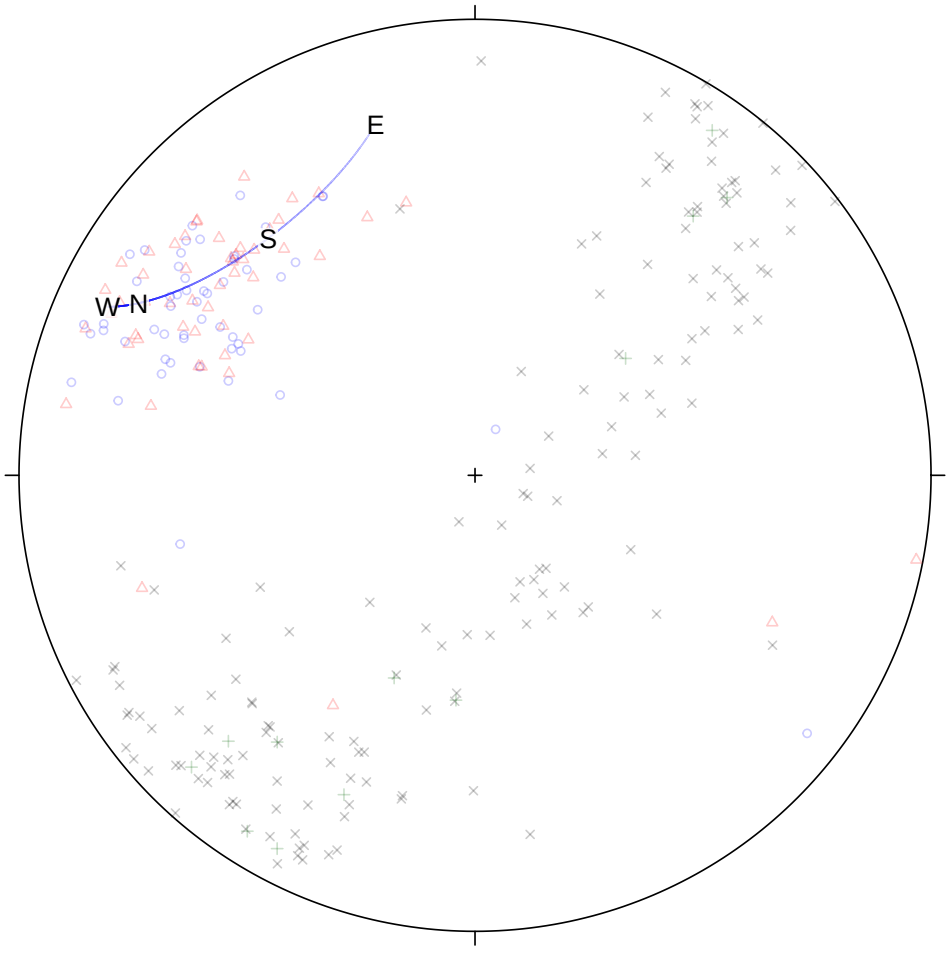

Figure 3.9 Stacked trend of the small circle model.

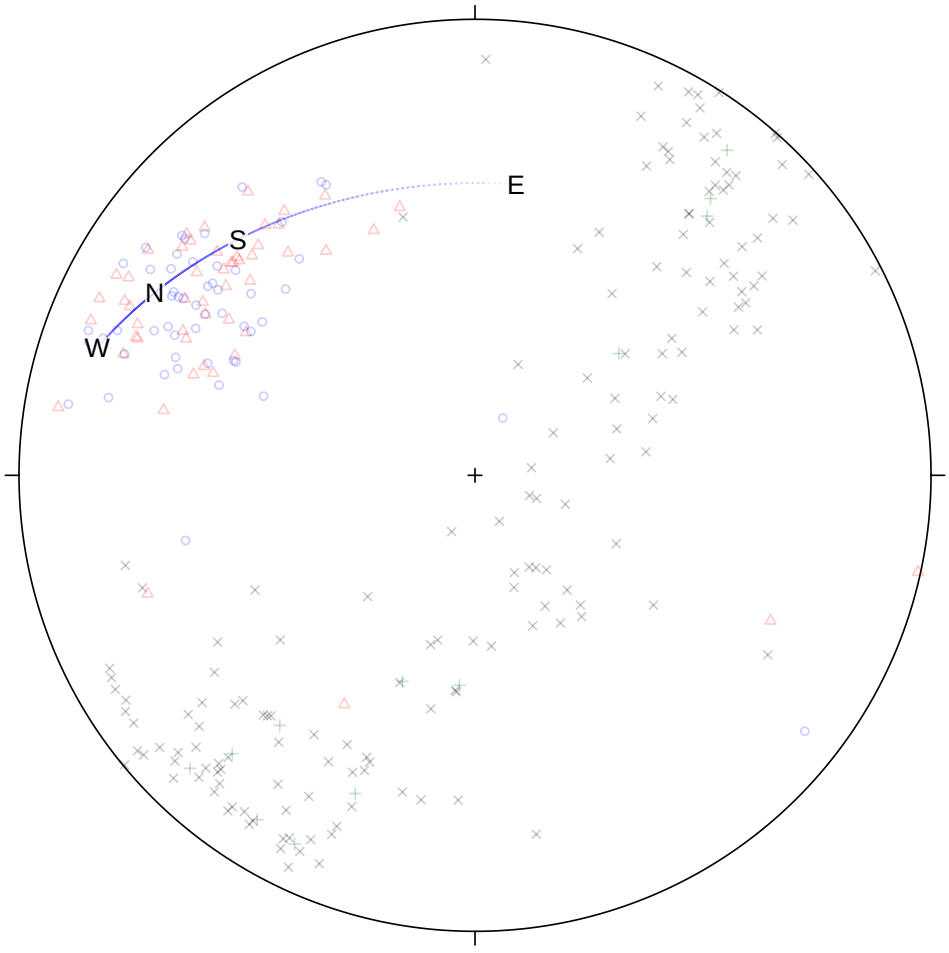

Figure 3.10 Stacked trend of the great circle model.

In the case of orientation data, residuals can be obtained by rotating predicted values together with observations to some "zero" orientation. For convenience of representation on stereonets I choose the "zero" to be $(0, 0, 1)$ (straight down).

Figures 3.11 through 3.14 show the residual plots for all four models. Each figure consist of two stereonets. One on the left hand side shows the residuals for the pooled estimator $\beta^{b,c}$. Green and blue clouds represent 100 times bootstrapped sample of the β axis estimations from b and c structures correspondingly. This stereonet is provided to aid comparison (bad vs. good).

The stereonet on the right displays the same information but for one of the four regression models.

The bootstrap clouds of the "full" and the small circle models are similar. Although they are much closer than the clouds of the pooled estimator residuals they are still separated. A precise answer to the question whether the directions of the β^b and β^c estimators are different or not should be given by statistical inference. Unfortunately this is a topic for another research. For now I will claim these estimators not to be significantly different and therefore the assumption of the orthogonality is valid.

In case of the great circle model the bootstrap clusters are strongly separated. The obvious reason for this is the failure to correctly estimate the spatial trend.

The "null" model never aimed to account for any trend, therefore the clouds are even farther apart. As mentioned before, this model is extremely close to the pooled estimator model.

Another important assumption implicit in the objective function (equation (2.20)) is the equality of the dispersion of b structures around the β axis to the dispersion of c structures with respect to a great circle normal to the β axis.

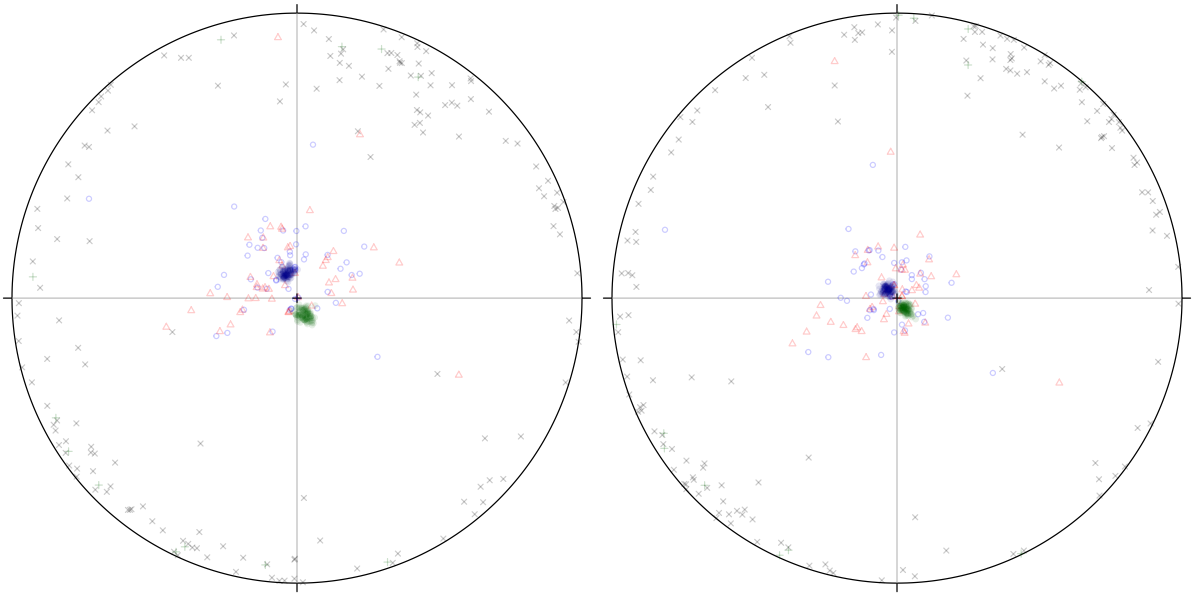

Figure 3.11 Plot of residuals from the "full" model and the bootstrap clouds (right plot) and the same for the pooled estimator (left).

The b structures are shown as circles and triangles and c fabrics as crosses. Thus the dispersions can be approximately assessed from the stereonets.

In my opinion these plots do not show any significant difference in variance of b- and c-structures.

As a conclusion, the model of choice for this data is the small circle model. It is almost as good as the "full" model in terms of the mean error, but since it has fewer parameters, it will have a better performance for unexisting inference procedures. Moreover it is much simpler for the geological interpretation. Unlike the "full" model, which is a nine-parameter vector field, the small circle model can be represented as a combination of a constant vector of rotation and a linear scalar field of the tangent of the rotation angle.

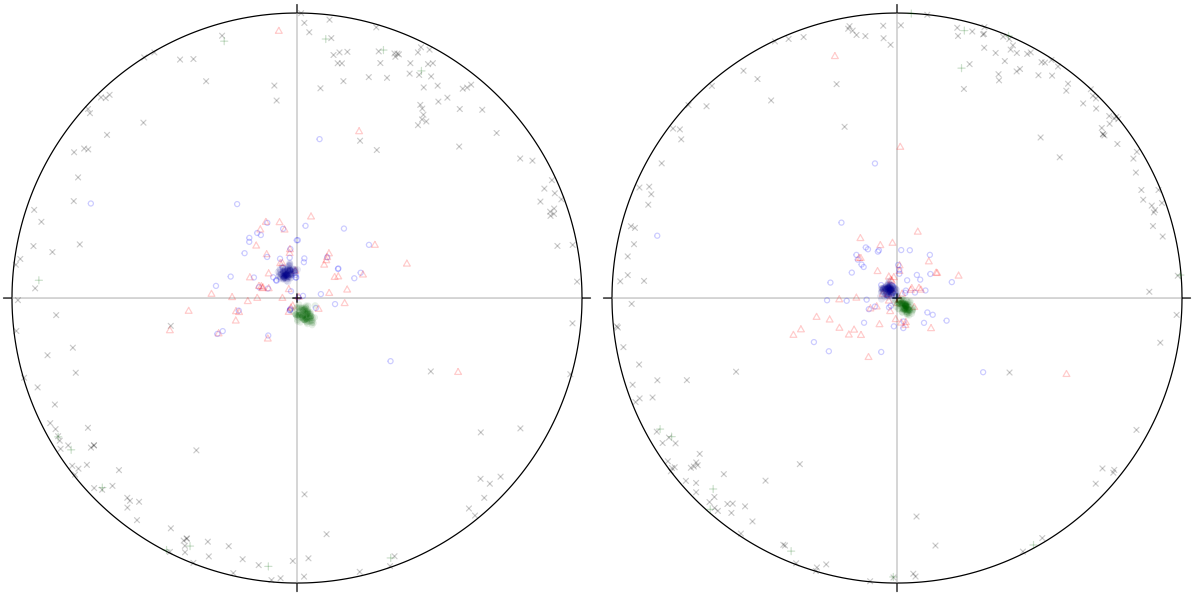

Figure 3.12 Plot of residuals from the small circle model and the bootstrap clouds (right plot) and the same for the pooled estimator (left).

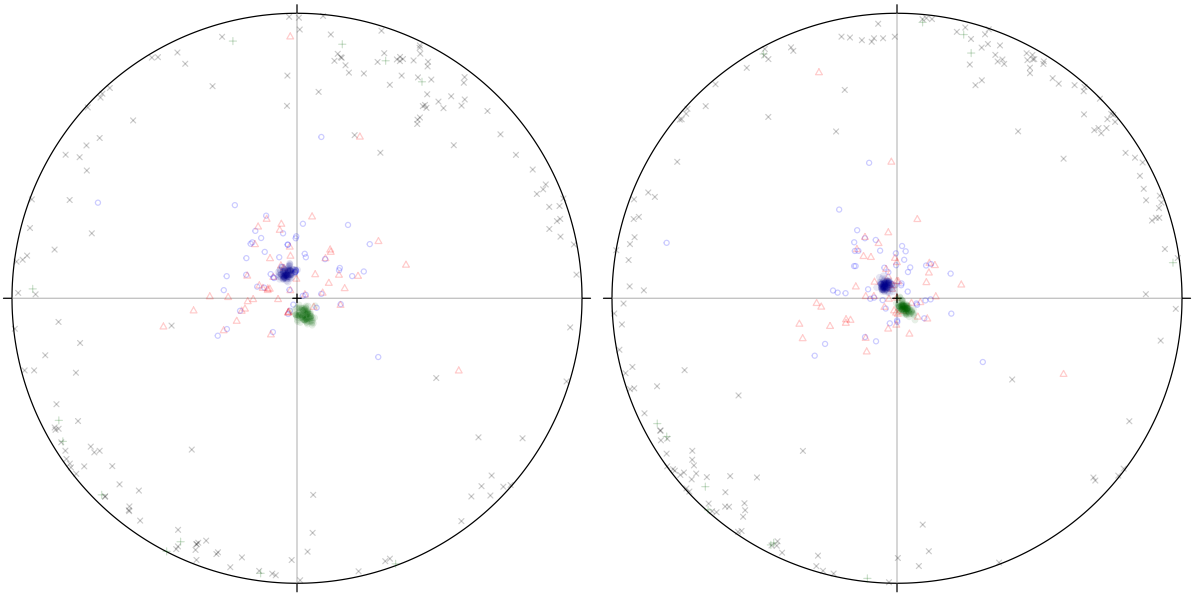

Figure 3.13 Plot of residuals from the great circle model and the bootstrap clouds (right plot) and the same for the pooled estimator (left).

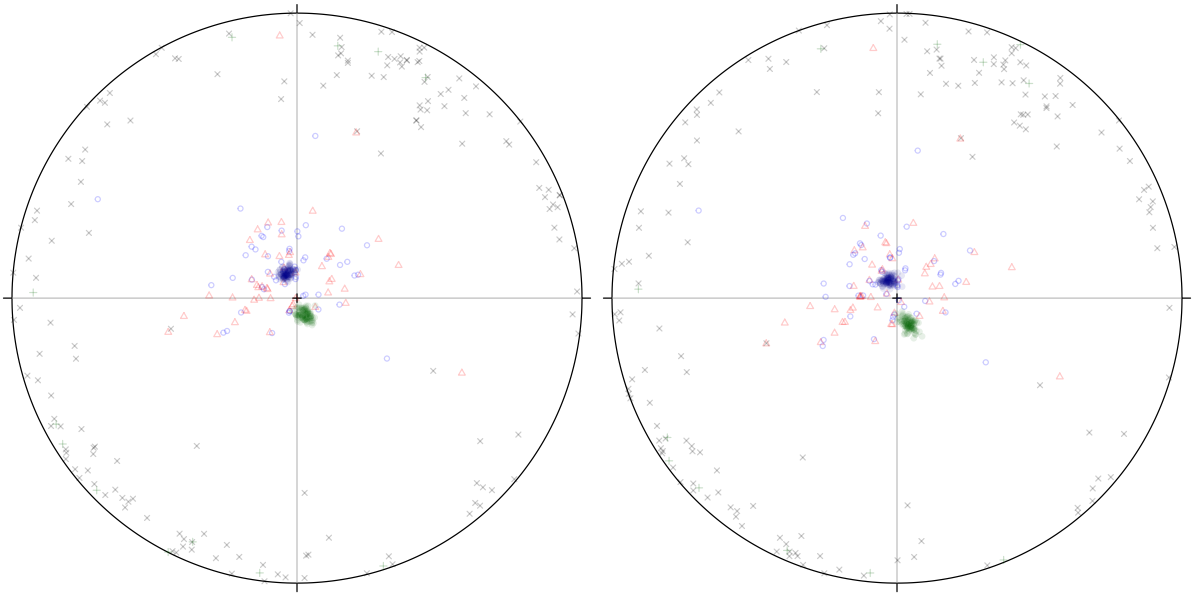

Figure 3.14 Plot of residuals from the "null" and the bootstrap clouds (right plot) and the same for the pooled estimator (left).

The great circle model does not fit the data particularly well. This is especially clear at the eastern part of the area where the predicted values of the β axis are way too over-rotated.

The "null" model is of zero interest. Here it was presented mostly for the completeness. However it will find its application in testing the hypothesis of no trend.

The overall reduction of the dispersion seen on figures 3.11–3.13 of the residuals of the first three models corresponds to the effect and the principal of the regression — minimization of the total error.

This residual dispersion is unexplained by the models variance which can be studied further. For example, the residuals can be used to fit a variogram to study spatial autocorrelation. This was briefly mentioned in section 2.4. With knowledge of the autocorrelation properties of the data, kriging for orientations described by Young (1987a,b)

and van den Boogaart & Schaeben (2002a,b) can be used to assess smaller scale variations.

Besides that, the residuals can be used to study the c-fabric distribution. This aspect was completely neglected during the trend fitting, but is an important part of the orientation analysis study.

3.5 Geological Interpretation

It was mentioned in the beginning of this chapter that a model of a curved craton may explain the curvature of the structure. It was also shown why transpression conditions should appear in this case.

The derived trend of about 60° does not correspond to the model provided by Robin & Cruden (1994). Therefore it can be said that this data does not support that model.

A more complete study of the orientations that would provide some basis for an interpretation of this structure would include a study of residuals obtained from a model of choice. The regression models discussed in this work are concerned about just one aspect of the data structure — spatial trend of the β-axis orientation. However, this is not the most critical part of the numerical model of a transpression zone. What is really significant, is the distribution of the c-fabrics after subtracting the β-trend, i.e. the residuals. This detrended c-fabric data can be used to estimate such parameters as deformation intensity, kinematic vorticity number, Flynn parameter and so forth. However, the goal of this work was not a study of the Kukas lake structure, but methods for this study. Therefore, no further analysis was done and no important conclusions about the structure can be drawn.

CHAPTER 4

CONCLUSIONS

This research is a continuation of research to develop statistical methods for orientation analysis in structural geology. Spherical data, one of the most important forms of information in structural geology, is significantly different from linear data which is the target of almost all statistical techniques developed to date. Although it is quite easy to transform orientation data into linear space, the inverse transformation is more challenging in terms of providing a surjective mapping. Almost all transformation based techniques suffer from this problem.

This paper presents a new (at least for the orientation data) transformation from a sphere to linear space by virtue of rotations and pseudo-vectors. Although this transformation is surjective, it is not injective, i.e. a single point in the original space corresponds to many points in the transformed space. However this does not seem to be a problem for the regression techniques based on this transformation as presented in this paper.

These methods are actually linear regression models of orientations in the transformed space on a spatial location with a special treatment for errors. Since the transformation is not injective, the errors have to be measured in the original space. Therefore the model formulae and the developed optimization technique look different from ones used in classical linear regression.

Another difference from a casual linear model is the use of two different sources of information. The proposed methods take advantage of having measurements of both b- and c-types of fabrics without requiring them to be paired. This is important when every bit of information is precious and no data can be discarded.

Four variants of this model are presented starting with the most comprehensive "full" model that includes nine parameters and is very flexible, but is also rather hard to interpret.

The next, small circle model, is a reduction of the "full" model, which restricts it to a constant axis of rotation. The great circle model is its further simplification with a restriction of the angle between the axis of rotation and the β axis to a given value ($\pi/2$ in this work). These models have the advantage of simplicity combined with moderate flexibility.

The last, "null" model is a model of no rotation whatsoever. This model is mostly reserved for future use, when methods of inference will be developed.

Besides these spatial trend models, a pooled estimator $\beta^{b,c}$ is also presented. Like the regression models, this estimator is designed to incorporate unpaired observations on different types of data. However this estimator disregards the spatial component, and in this sense is somewhat similar to the "null" model.

Examples of all these techniques are given using the data from the Kukas lake structure of the Baltic shield. The methods found and quantified a trend in orientation of the β-axis allowing a further study of residuals that would give estimations necessary for comparison with numeric models.

It is shown that the residuals obtained from the fitted models can be used for further analysis using geostatistics.

The main direction for further research should be development of inferential techniques. One of the simpler approaches would be bootstrapping. Indeed the distribution theory for orientation data is quite difficult. Moreover, most of the geological data is spatially attributed, therefore it is highly possible that it is autocorrelated, which means that the traditional maximum likelihood methods will not be suitable.

All computations were done using the R language (R Development Core Team, 2005). A set of functions was created, which will be published at the CRAN (Comprehensive R Archive Network) web site as a stand alone package.

REFERENCES

Altmann, S. L. (1986). *Rotations, Quaternions, and Double Groups*. Clarendon Press, Oxford.

Beran, R. (1979). Exponential models for directional data. *The Annals of Statistics* 7 1162–1178.

Bingham, C. (1974). An antipodally symmetric distribution on the sphere. *The Annals of Statistics* 2 1201–1225.

Bingham, C., Chang, T. & Richards, D. (1992). Approximating the matrix Fisher and Bingham distributions : Applications to spherical regression and procrustes analysis. *Journal of Multivariate Analysis* 41 314–337.

Bingham, C. & Mardia, K. V. (1978). A small circle distribution on the sphere. *Biometrika* 65 379–389.

Bowman, A. W. & Azzalini, A. (1997). *Applied smoothing techniques for data analysis : the kernel approach with S-Plus illustrations*, vol. 18. Oxford: Clarendon Press.

Chilès, J.-P. & Delfiner, P. (1999). *Geostatistics : modeling spatial uncertainty*. Wiley series in probability and statistics. Applied probability and statistics. New York: Wiley.

Cressie, N. A. C. (1993). *Statistics for spatial data*. Wiley series in probability and statistics. Applied probability and statistics. New York: Wiley.

de Waal, D. J. (1979). On the normalizing constant for the Bingham-von Mises-Fisher matrix distribution. *South African Statist. J.* 13 103–112.

Downs, T. D. (1972). Orientation statistics. *Biometrika* 59 665–676.

Ducharme, G. R. (1985). Bootstrap confidence cones for directional data. *Biometrika* 72 637–645.

Ducharme, G. R. & Milasevic, P. (1987). Spatial median and directional data. *Biometrika* 74 212–215.

Duda, R. O., Hart, P. E. & Stork, D. G. (2000). Pattern classification.

Fisher, N. I. & Hall, P. (1989). Bootstrap confidence regions for directional data. *Journal of the American Statistical Association* 84 996–1002.

Fisher, N. I., Hall, P., Jing, B.-Y. & Wood, A. T. A. (1996). Improved pivotal methods for constructing confidence regions with directional data. *Journal of the American Statistical Association* 91 1062–1070.

Fisher, N. I., Lewis, T. & Embleton, B. J. J. (1993). *Statistical analysis of spherical data*. Cambridge University Press.

Griffith, D. A. (1988). *Advanced spatial statistics : special topics in the exploration of quantitative spatial data series*, vol. 12. Dordrecht; Boston: Kluwer Academic Publishers.

Haining, R. P. (2003). *Spatial data analysis : theory and practice*. Cambridge, UK ; New York: Cambridge University Press.

Hallin, M., Lu, Z. & Tran, L. T. (2004). Kernel density estimation for spatial processes: the l1 theory. *Journal of Multivariate Analysis* 88 61–75.

Hanmer, S. & Passchier, C. W. (1991). *Shear-sense indicators : a review*, vol. 90-17. Ottawa, Canada: Energy, Mines, and Resources Canada : Geological Survey of Canada distributor.

Houlding, S. W. (2000). *Practical Geostatistics : Modelling and Spatial Analysis*. Berlin: Springer Verlag.

Jupp, P. E. (1987). A nonparametric correlation coefficient and a two-sample test for random vectors or directions. *Biometrika* 74 887–890.

Jupp, P. E. & Mardia, K. V. (1979). Maximum likelihood estimators for the matrix von Mises-Fisher and Bingham distributions. *The Annals of Statistics* 7 599–606.

Jupp, P. E. & Mardia, K. V. (1980). A general correlation coefficient for directional data and related regression problems. *Biometrika* 67 163–173.

Jupp, P. E. & Mardia, K. V. (1989). A unified view of the theory of directional statistics, 1975–1988. *International Statistical Review* 57 261–294.

Jupp, P. E. & Spurr, B. D. (1983). Sobolev tests for symmetry of directional data. *The Annals of Statistics* 11 1225–1231.

Karato, S. & Wenk, H.-R., eds. (2002). *Plastic deformation of minerals and rocks*, vol. 51. Washington: Mineralogical Society of America.

Kent, J. T. (1982). The fisher-bingham distribution on the sphere. *Journal of the Royal Statistical Society. Series B (Methodological)* 44 71–80.

Kent, J. T. (1987). Asymptotic expansions for the bingham distribution. *Applied Statistics* 36 139–144.

Khatri, C. G. & Mardia, K. V. (1977). The von Mises-Fisher matrix distribution in orientation statistics. *Journal of the Royal Statistical Society. Series B (Methodological)* 39 95–106.

Kunze, K. & Schaeben, H. (2004). The Bingham distribution of quaternions and its spherical radon transform in texture analysis. *Mathematical Geology* 36 917–943.

Lisle, R. J. (1985). The use of the orientation tensor for the description and statistical testing of fabrics. *Journal of Structural Geology* 7 115–117.

Mardia, K. V. (1975). Statistics of directional data. *Journal of the Royal Statistical Society. Series B (Methodological)* 37 349–393.

Mardia, K. V. & Jupp, P. E. (2000). *Directional statistics*. New York: Wiley.

Nicolas, A. (1987). *Principles of rock deformation*. Dordrecht: Reidel.

Prentice, M. J. (1978). On invariant tests of uniformity for directions and orientations. *The Annals of Statistics* 6 169–176.

Prentice, M. J. (1984). A distribution-free method of interval estimation for unsigned directional data. *Biometrika* 71 147–154.

Presnell, B., Morrison, S. P. & Littell, R. C. (1998). Projected multivariate linear models for directional data. *Journal of the American Statistical Association* 93 1068–1077.

Purkayastha, S. & Mukerjee, R. (1992). Maximum likelihood characterization of the von Mises-Fisher matrix distribution. *Sankhyā (Statistics). The Indian Journal of Statistics. Series A* 54 123–127.

R Development Core Team (2005). *R: A language and environment for statistical computing*. R Foundation for Statistical Computing, Vienna, Austria.

Ripley, B. D. (2004). *Spatial statistics*. Hoboken, N.J.: Wiley-Interscience.

Rivest, L.-P. (1989). Spherical regression for concentrated Fisher-von Mises distributions. *The Annals of Statistics* 17 307–317.

Rivoirard, J. (1994). *Introduction to disjunctive kriging and non-linear geostatistics*. Oxford ; New York: Oxford University Press.

Robin, P.-Y. F. & Cruden, A. R. (1994). Strain and vorticity patterns in ideally ductile transpression zones. *Journal of Structural Geology* 16 447–466.

Schabenberger, O. & Gotway, C. A. (2005). *Statistical methods for spatial data analysis*. Boca Raton: Chapman & Hall/CRC.

Somin, M. L. & Travin, V. V. (2002). On Sumii quartzites and nature of the Kukas lake structure of the Baltic shield. *Doklady Akademii Nauk* 382 92. In Russian.

Travin, V. V. (1992). Dynamic nature of a zone of apparent lineation of the east kukas lake region. In *Voprosy Geologii i Magmatizma Dokembrija Karelii*. Petrozavodsk: KSC RAS, 21–26. In Russian.

Turner, F. J. & Weiss, L. E. (1963). *Structural analysis of metamorphic tectonites*. New York: McGraw-Hill.

Tyler, D. E. (1987). Statistical analysis for the angular central gaussian distribution on the sphere. *Biometrika* 74 579–589.

Upton, G. J. G. & Fingleton, B. (1985). *Spatial data analysis by example*. Chichester; New York: Wiley.

van den Boogaart, K. G. & Schaeben, H. (2002a). Kriging of regionalized directions, axes, and orientations I: Directions and axes. *Mathematical Geology* 34 479–503.

van den Boogaart, K. G. & Schaeben, H. (2002b). Kriging of regionalized directions, axes, and orientations II: Orientations. *Mathematical Geology* 34 671–677.

Vollmer, F. W. (1990). An application of eigenvalue methods to structural domain analysis. *Geological Society of America Bulletin* 102 786–791.

Watson, G. S. (1983). *Statistics on spheres*, vol. 6 of *University of Arkansas Lecture Notes in the Mathematical Sciences*. New York: Wiley.

Wellner, J. A. (1979). Permutation tests for directional data. *The Annals of Statistics* 7 929–943.

Wood, A. T. A. (1982). A bimodal distribution on the sphere. *Applied Statistics* 31 52–58.

Wood, A. T. A. (1987). The simulation of spherical distributions in the fisher-bingham family. *Communications in statistics* 16 885–898.

Wood, A. T. A. (1993). Estimation of the concentration parameters of the Fisher matrix distribution on SO(3) and the Bingham distribution on $S_q,\ q \geq 2$. *The Australian Journal of Statistics* 35 69–79.

Woodcock, N. H. (1977). Specification of fabric shapes using an eigenvalue method. *Geological Society of America Bulletin* 88 1231–1236.

Young, D. S. (1987a). Indicator kriging for unit vectors : rock joint orientations. *Mathematical Geology* 19 481–501.

YOUNG, D. S. (1987b). Random vectors and spatial analysis by geostatistics for geotechnical applications. *Mathematical Geology* 19 467–480.

BIOGRAPHICAL INFORMATION

Boris Avdeev was born in Leningrad, USSR, in 1980. He received his B.S. degree in Geology from St. Petersburg State University, Russia, in 2001. From 2003 until now, he has been working on his Master's degree at the Geology Department of the University of Texas at Arlington.